Trace elements in PM$_{2.5}$ aerosols in East Asian outflow in the spring of 2018: Emission, transport, and source apportionment

Takuma Miyakawa[1], Akinori Ito[1], Chunmao Zhu[1], Atsushi Shimizu[2], Erika Matsumoto[3], Yusuke Mizuno[3], Yugo Kanaya[1]

[1]Research Institute for Global Change, Japan Agency for Marine-Earth Science and Technology, Yokohama, 236-0001, Japan

[2]Regional Environment Conservation Division, National Institute for Environmental Studies, Tsukuba, 305-8506, Japan
[3]Horiba Ltd., Ohtsu, 520-0102, Japan

Correspondence to: Takuma Miyakawa (miyakawat@jamstec.go.jp)

Abstract. Trace metals in aerosol particles impact Earth's radiative budget, human health, and ocean biogeochemistry. Therefore, sSemi-continuous measurements of the elemental composition of fine mode (PM$_{2.5}$) aerosols were conducted using an automated X-ray fluorescence analyzer on a remote island of Japan during the spring of 2018. The temporal variations of in mass concentrations of geochemically important elements for this period, such as S, Pb, Cu, Si, Fe, and FeMn, and their relationships with the emission tracers, carbon monoxide (CO) and black carbon (BC), were reported. The Integrated Massively Parallel Atmospheric Chemical Transport (IMPACT) model was used to evaluate the source apportionment of these components and was evaluated in terms of emissions and wet removal processes. Pb and Cu were found to have originated mainly from anthropogenic sources (98% and 93% on average, respectively) over the East Asian continent. A pPositive correlations of Pb and Cu with BC and CO and the similarity of their concentration-weighted trajectories was found during the study period, indicating indicated that the emission sources of these metals share the region where the large CO (and BC) emission sources are located and that CO can be regarded as a tracer of the continental anthropogenic emissions. The air masses with minimized impacts of the wet removal during the transport were extracted to elucidate the "top-down" emission ratio of Pb and Cu to CO, which were, for the first time, evaluated as 152.7 and 63.1 µg g^{-1}, respectively, during the spring of 2018 in the East Asian outflow. The analysis of the tagged tracer simulations by the IMPACT model confirmed that BC and Si can could be used as tracers for anthropogenic and dust emissions, respectively, during the observation period. The source apportionment of Fe and Mn in PM$_{2.5}$ aerosols was conducted using Si and BC tracers, which revealed that the anthropogenic contribution was 17% and 44% on average, respectively. Based on the air mass origins of Fe and Mn, their anthropogenic fraction varied from 2% to 29% and 9% to 68%, respectively, during the high PM$_{2.5}$ concentration periods. However, despite the minor non-dominant anthropogenic contributions of Fe, they can could adversely affect human health and ocean biogeochemistry owing to their higher water solubility. The modeled BC, Pb, Cu, and Fe were evaluated by separately diagnosing their emission and transport. Ratios of modeled to observed concentrations for these components were analyzed in terms of the accumulated precipitation along the transport from the East Asian continent. The current model simulations were found to overestimate the emissions (based on Community Emissions Data System, CEDS v2021-02-05) of BC by 44% and

underestimate Cu by 45%, anthropogenic Fe by 28% in East Asia, and the wet deposition rates for BC and Pb. Overall, Cu in East Asia exhibited a different nature from BC and Pb in terms of emission sources and wet removal.

1 Introduction

Aerosol particles play essential roles in the atmosphere, as they affect Earth's radiative balance (Szopa et al., 2021 and references therein), human health (e.g., Pope and Dockery, 2006), and ocean biogeochemistry (e.g., Tagliabue et al., 2017). The significance of metallic elements in aerosol particles is in debate, even though their contribution to total aerosol masses or aerosol optical depth is not always dominant in ~~a wide variety of~~various atmospheric environments (Myhre et al., 2013). Recent studies suggest that airborne anthropogenic iron oxides (FeO_X) (e.g., magnetite) particles efficiently absorb solar radiation and pose a significant impact ~~on~~ to the regional radiative forcing (Ito et al., 2021; Lamb et al., 2021; Moteki et al., 2017). Transition metals in fine particles, such as Cu, Mn, and Fe, have strong impacts on the formation of reactive oxygen species (ROS) in cells (e.g., Charrier and Anastasio, 2012). The oxidative potential of aerosol particles, which have the potential to generate ROS in cells and cause oxidative stress to cells, has been a concern~~ed~~. Using the mass concentrations of the $PM_{2.5}$ aerosols (particulate matter with an aerodynamic diameter smaller than 2.5 µm) obtained from more than 60 sites worldwide, Lakey et al. (2016) demonstrated a model simulation of ROS production in the epithelial lining fluid (ELF) and showed that the ROS concentrations in the ELF increase with the increase in ~~the~~ $PM_{2.5}$ concentrations. They further suggested that the ROS concentrations greatly vari~~ed~~es at the same levels as the $PM_{2.5}$ concentrations, and that this variability ~~is~~ was attributed to the constituents of the $PM_{2.5}$ aerosols, such as transition metals and organics. In the ocean biogeochemical cycles, Fe and Mn play a role as growth-limiting nutrients for ~~the~~ marine phytoplankton in the high nitrate, low chlorophyll (HNLC) regions such as the northwestern Pacific Ocean and Southern Ocean, and the leachable fraction of Fe is a key to assessing the bioaccessibility of Fe in the surface seawater (Mahowald et al., 2018 and references therein). Some other trace metals can limit microbial biogeochemistry (e.g., Zn, Co, and Mn; Moore et al., 2013), and their higher concentrations can be toxic to some plankton (e.g., Cu; Jordi et al., 2012; Yang et al., 2019). This indicates that atmospheric depositions of these trace metals onto the ocean surface can alter the community composition and potentially inhibit biological productivity.

Asia is recognized as one of the massive anthropogenic emission regions of metallic aerosols (Pacyna and Pacyna, 2001). The concentration levels of trace metals in the East Asian outflow have been characterized in some islands facing the Sea of Japan during 1988–1990 (Mukai and Suzuki, 1996) and the East China Sea during 2012–2014 (Shimada et al., 2018). These studies suggested that the metal concentrations are elevated in the air masses transported from the continent, while they are lowest in the summer when the background air masses are frequently advected from the Pacific Ocean. Mukai and Suzuki (1996) used monthly mean data sets of almost three years (1988–1990), and reported the importance of the effects of precipitation on the transboundary transport of metallic elements, especially in fine mode aerosols, through the wet removal processes. They did not rigorously investigate the impacts of the wet removal ~~along~~ during~~the~~ transport from the source regions due to technical data limitations (e.g., longer-time filter sampling and the following chemical analyses). The wet removal of black carbon (BC)

aerosols originating from combustion sources has been investigated using high-temporal resolution measurements of BC and carbon monoxide (CO), which is inert against wet removal processes and thereby considered a reliable tracer for the combustion sources (Choi et al., 2020; Kanaya et al., 2016; Verma et al., 2011). They suggested that the transport efficiency of BC from the continent to the outflow varied according to the air mass histories (e.g., transport altitude below or above the cloud, strength of the precipitation during the transport, etc.). A recent study revealed the decadal decreasing trends (2009–2019) of total $PM_{2.5}$ and BC aerosol concentrations in East Asian outflow, which can be attributed to the rapid reduction of anthropogenic emissions in China (Kanaya et al., 2020). ~~Since~~ Because atmospheric concentrations of metallic aerosols emitted from combustion sources are expected to be reduced, further studies are urgently needed on recent concentration levels with high temporal resolution (e.g., Fang et al., 2015; Liu et al., 2019) and their atmospheric behaviors such as transport and removal (e.g., Yoshida et al., 2020) to understand the responses of metallic aerosols in East Asia to the emission regulations and predict future climate change affecting atmospheric transport.

Modeling attempts for the simulation of the multi-elemental compositions of atmospheric aerosols have been challenging. Only limited studies have tackled this issue, especially in East Asia (Chatani et al., 2021; Kajino et al., 2020; 2021). The Integrated Massively Parallel Atmospheric Chemical Transport Model (IMPACT; e.g., Ito et al., 2023) ~~has the capability to~~can accurately simulate the concentrations of Fe aerosols and the variations in its bioacessibility by considering the chemical aging process. Recently, the IMPACT model was refined to simulate the multi-elemental compositions of atmospheric aerosols, and the IMPACT model was evaluated in terms of its global scale applicability in a previous study (Ito and Miyakawa, 2023).

The conventional way to accurately quantify the elemental compositions, for example, by Inductively-coupled plasma mass spectrometry (ICP-MS), requires large-volume air sampling and time- and cost-consuming destructive pretreatment steps for the analyses. Unlike ICP-MS, the X-ray fluorescence (XRF) technique has the benefit of easily conducting non-destructive analysis of many samples. ~~Continuous~~ A continuous Particulate Monitor with the XRF analysis (PX-375) has been developed by Horiba Ltd. (Asano et al., 2017). In this study, to investigate the emission and transport of trace metals in $PM_{2.5}$ aerosols from the East Asian continent, PX-375 was deployed on Fukue Island (Kanaya et al., 2016; 2020; Miyakawa et al., 2017; 2019) in the spring (March–April–May) of 2018. Furthermore, collocated measurements of BC and CO concentrations (Kanaya et al., 2016) were integrated into the detailed data analyses to investigate the emission and transport of targeted metallic elements. The IMPACT model was evaluated in terms of emission and transport of the targeted metallic elements in $PM_{2.5}$ aerosols, and was used to investigate the source apportionment of metals in East Asian outflow based on tagged tracer simulation results.

2 Material and methods

2.1 Observations

Continuous measurement of trace gases and $PM_{2.5}$ aerosols has been conducted at Fukue Island, which is a remote island in western Japan, since February 2009 (Kanaya et al., 2016). The observation site was located at the Fukue Island Atmospheric

Environment Monitoring Station (Fukue site; 32.75° N, 128.68° E). The mixing ratio of CO was measured using a nondispersive infrared (NDIR) CO monitor (model 48C, Thermo Scientific, Inc., USA), and mass concentrations of fine particles ($PM_{2.5}$) and BC were measured using a Synchronized Hybrid Ambient Real-time Particulate (SHARP) monitor

100 (model 5030, Thermo Scientific, Inc., USA) and Multi Angle Absorption Photometer (MAAP, model 5012, Thermo Scientific, Inc., USA), respectively. According to the intercomparison studies between MAAP and other independent instruments (Kanaya et al., 2013; 2016; Miyakawa et al., 2019)), the mass absorption cross section for the MAAP was modified from the manufacturer's recommendation of 6.6 to 10.3 $m^2\,g^{-1}$. The BC observations using the MAAP were evaluated by a Single Particle Soot Photometer (SP2; Droplet Measurement Technologies, Longmont, Colorado, USA) (Miyakawa et al., 2019).

105 Details of the CO and $PM_{2.5}$ measurements are outlined in Kanaya et al. (2016; 2020), some of which revealed that the elevated concentrations of CO, BC, and $PM_{2.5}$ at the observation site were mainly affected by the transboundary transport of polluted air masses from the Asian continent (i.e., long-range transport) with negligible impact of local emission sources (e.g., Kanaya et al., 2016).

Elemental compositions of $PM_{2.5}$ aerosols were measured using a Continuous Particulate Monitor with the XRF analysis (PX-

110 375, Horiba Ltd., Kyoto, Japan). The instrumental design is described in Asano et al. (2017). However, the instrument can be briefly described as follows: PX-375 consists of a collection unit for aerosol particles on a filter, the measurement unit for the mass of the collected aerosol particles, and an XRF analysis chamber; the filter tape used for the particle collection was fabricated by Horiba Ltd. (TFH-01, Horiba Ltd.); and TFH-01 is a polytetrafluoroethylene (PTFE) filter with non-woven fabric polyethylene (PE) and polyethylene terephthalate (PET) backing, which was designed to mechanically strengthen the

115 filter structure. The total mass of $PM_{2.5}$ aerosols collected on the filter was analyzed using a radiocarbon-based beta-ray attenuation method during the particle collection. The 4 hourly $PM_{2.5}$ mass concentrations measured using the PX-375 were compared with those measured using the SHARP monitor. PX-375-derived $PM_{2.5}$ mass concentrations were found to be in good agreement (within 10%) with those observed by the SHARP monitor. After sampling, a particle-laden spot on the filter was transferred into the XRF analysis chamber by advancing the filter roll tape and then analyzed by the XRF technique. The

120 ambient air was drawn at 16.7 liters per minute through the $PM_{2.5}$ cyclone (URG-2000-30EH, URG Corp., North Carolina, USA) into the PX-375 instrument. During the observation period, the $PM_{2.5}$ aerosol particles were collected for 4 h, and the XRF analyses were performed with 4000 sec of X-ray irradiation at 15 and 50 kV. The typical volume of the sampled air was 4 m^3 per particle-laden spot. The limits of detection (LODs) were evaluated by repeated measurements placing the high efficiency particulate air (HEPA) filter in front of the PX-375 to introduce particle-free air into the PX-375. The LODs were

125 defined as three times the standard deviations of the measured values by the PX-375 at the observation site and were evaluated to be 1.57, 0.28, 0.70, 0.69, 25.6, 18.3, 1.95, 8.50, and 9.50 ng m^{-3} for Fe, Pb, Cu, Mn, K, Cl, Ca, Si, and S as sulfate, respectively. The particle-laden spots on the filter roll tape were cut into pieces after the observation period and then stored in the refrigerator (at approximately −20 °C). The particle spots can be reanalyzed by different techniques (e.g., Zhu et al., 2021). In this study, particle spots collected before ~~this~~ these observations were reanalyzed for the recalibrations of the onsite

130 measurements using different chemical analysis techniques: ion chromatography (IC) for Cl (as chloride) and S (as sulfate)

and ICP-MS for Fe, Pb, Mn, Cu, Mn, K, and Ca. ~~Considering~~ Based on the intercomparison results (linear regression slopes and their variances), the relative errors ~~uncertainties~~ in the on-site measurements of the concentrations of Cl, S, Fe, Pb, Mn, Cu, K, and Ca were evaluated to be 66%, 6%, 26%, 15%, 23%, 30%, 28%, and 33%, respectively.

Lidar-derived aerosol extinction coefficients at 532 nm (e.g., Shimizu et al., 2015) were analyzed to investigate the impacts of
135   Asian dust on the measured aerosol concentrations. The lidar measurements at the same site were part of the lidar network over Asia and are maintained by the National Institute for Environmental Studies in Japan (Shimizu et al., 2004; Sugimoto et al., 2003). The contribution of dust to the lidar-derived aerosol extinction coefficient was estimated using the aerosol depolarization ratio, assuming that dust particles are externally mixed with spherical particles. All the lidar data were obtained with 15 min temporal and 30 m vertical resolutions. The dust aerosol extinction coefficients near the surface were estimated
140   by averaging the dust extinction coefficients between heights of 120 and 240 m (the contribution below 120 m was not measured and, thereby, was omitted in this study) and were merged into 4 hourly elemental composition datasets. Note that the lidar measured the particles for the whole size range, including coarse particles (>2.5 μm in diameter), unlike the in-situ measurements using the PX-375.

2.2 Meteorological data and air mass origin analyses

145   Backward trajectories were calculated from the observation site to elucidate the impact of Asian outflow. ~~Five day~~Five-day backward trajectories from the observation site (at a starting altitude of 0.5, 1.0, and 1.5 km) were calculated every hour using the NOAA Hybrid Single-Particle Lagrangian Integrated Trajectory Model (Draxler and Rolph, 2012; Rolph, 2012; Stein et al., 2015) with the meteorological data sets with a resolution of 1° in latitude and longitude (NCEP's GDAS). The accumulated precipitation along trajectories (APT) for three days before the measurement was calculated to discuss the wet removal during
150   transport (Kanaya et al., 2016; Miyakawa et al., 2017). The concentration-weighted trajectory (CWT) for a pollutant in a particular grid of latitude and longitude (i, j) was measured to determine the pollutant source strength in a grid of a receptor site. In this study, this analysis was applied to the four hourly aerosol mass concentrations observed at the observation site. The CWT for the aerosol concentrations was determined as follows (Kabashnikov et al., 2011):

155
$$CWT_{i,j} = \left. \sum_{k=1}^{L}\left(C_k \cdot \tau_{i,j,k}\right) \middle/ \sum_{k=1}^{L} \tau_{i,j,k} \right.$$
(Eq. 1)

where C_k is the mass concentrations of total and selected contents in $PM_{2.5}$ aerosols corresponding to the arrival of backward trajectory k; $\tau_{i,j,k}$ is the residence time of trajectory segment endpoints in the grid cell (latitude i and longitude j) for backward trajectory k; and L is the total number of backward trajectories (6600).

160   Since the 4 hourly concentrations are discussed in this study, the same values of C_k for hourly-calculated backward trajectories for a 4 ~~hour~~ duration were used for calculating the CWT. The resolution of a grid cell was 1° in latitude and longitude. $\tau_{i,j,k}$ was determined by counting the number of the calculated hourly trajectory segment endpoints only below 2 km altitude in

each grid cell for each trajectory. The reason for limiting the altitude for counting backward trajectories to below 2 km was to investigate the impact of the surface emission sources over the land area.

2.3 Integrated Massively Parallel Atmospheric Chemical Transport Model

In this study, the IMPACT model (Ito and Miyakawa, 2023; and references therein) was deployed to simulate three-dimensional distribution of the atmospheric composition including targeted aerosol species, such as Fe. Ito and Miyakawa (2023) modified the IMPACT model to expand its capability to simulate ~~various~~ elements other than Fe, including Pb, Cu, Mn, and Si. They improved the IMPACT model to include metal smelting as an emission source of Fe, which has not well been evaluated in previous studies. The simulated atmospheric constituents of CO, BC, sulfate, Pb, Cu, Mn, and Fe concentrations were compared with the observations of this study. Source apportionment of trace elements in $PM_{2.5}$ aerosols was also analyzed based on the tagged tracer simulations using the IMPACT model, which ~~has a capability to~~can separately simulate lithogenic (i.e., mineral dust), pyrogenic (i.e., biomass burning), and anthropogenic (combustion and non-combustion) contributions of the selected species such as sulfate, BC, and Fe in $PM_{2.5}$ aerosols. A brief description of the IMPACT model related to BC and the trace metals is as follows:

The model simulations were performed using a horizontal resolution of $2.0° \times 2.5°$ (latitude × longitude) and 47 vertical layers. An emission inventory, Community Emissions Data System (CEDS, v-2021-02-05, O'Rourke et al., 2021), was used for fine particulate matter and BC emitting from anthropogenic sources. The metal content of $PM_{2.5}$ aerosols from lithogenic, pyrogenic, and anthropogenic sources was obtained from the compilation of source-specific aerosol measurements (Ito et al., 2018; Kajino et al., 2020; Reff et al., 2009). ~~Since~~ Because CEDS does not include the emission of BC (a combustion source tracer) from the metal production sector (e.g., the production of iron and steel, aluminum, and other non-ferrous metals), Fe emissions from the metal production sector was estimated by scaling sulfur dioxide (SO_2) emission from CEDS based on the relative emissions of Fe to SO_2 (Rathod et al., 2020) in each country. The simulation with the low estimate of smelting Fe emission factors showed the best agreement with the observations at the Fukue site, suggesting efficient and effective air quality management control strategies ~~of air quality management~~ for the smelting facilities in East Asia (Ito and Miyakawa, 2023). Thus, we did not consider the smelting sources for other elements in the base version of the IMPACT model. Nevertheless, the filtering units ~~have~~ only have a certain efficiency, leading to an avoidable release of air pollutants from the smelting facilities (e.g., Barcan, 2002; Sorooshian et al., 2012). In this study, the concentrations of Cu emitted from the Cu smelting sources ($Cu_{CuSmelt}$) were estimated ~~by~~in the following way. We calculated the averages of Cu content (11.35 ± 6.53 wt.%) and Fe content (1.37 ± 0.47 wt.%) in stack particulates emitted from three Cu smelters (Skeaff et al., 2014), and then used their ratio, $(Cu/Fe)_{CuSmelt}$, of ~~8.31 wt.%~~ 8.31 wt.%$^{-1}$, as a scaling factor to estimate the $Cu_{CuSmelt}$ concentrations ~~from~~using the Fe emissions from the Cu smelting sources in the improved version of the IMPACT model. Note that the resuspended road dust from mechanically generated tire or brake wear, which can be an important non-combustion source of Cu, is not explicitly simulated by the IMPACT model.

195   -The IMPACT model simulated the wet removal processes through the in-cloud (e.g., Ito and Xu et al., 2014) and below-cloud scavenging (Ito et al. and Kok, 2017). All the metal components are removed asat the same rates as BC (i.e., no differences in the removal efficiencies among elements in anthropogenic aerosols) in the model simulations, assuming internal mixing of BC and trace elements (e.g., Ito and Feng, 2010), which will be discussed in the later section.

3 Results and discussion

3.1 Meteorology

200   During the spring season, typical meteorological conditions in East Asian outflow were reported in our previous studies (Kanaya et al., 2016; Miyakawa et al., 2017; 2019). The mid-latitude region (35–50° N, 120–140° E) in East Asia is influenced by a modest monsoonal northwesterly flow from the continent to the observation area, while whereas the subtropical region (20–30° N, 110–130° E) is influenced by a persistent southwesterly flow, part of which converges into the observation area,
205   confluent with the north westerlies from the continent. As the low-level southerly flow transports warm and moist air into the observation area to sustain a large amount of precipitation, the transport efficiency of aerosol particles in these air masses is low due to wet removal. These similar transport patterns were observed in the spring of 2018 (**Figure S1**). From March to May 2018, the air masses were frequently transported directly from the East Asian continent (not via mainland Japan) to the observation site on Fukue Island, with small Japanese emission impacts (**Figure S2**). The APT had no distinct seasonal
210   progressions in the spring of 2018 and had no correlation with the residence time over the continent (**Figure S3**). Thus, there was no significant bias of air mass origins and pathways with respect toconcerning the data selection of air masses with non-zero or zero APT.Notably, air masses with and without substantial impacts from wet depositions were observed during the observation period.

3.2 Springtime PM$_{2.5}$ aerosols in the East Asian outflow in 2018

215   The temporal variations of PM$_{2.5}$ aerosols, sulfate, Si, Fe, Ca, Mn, Pb, Cu, BC, and CO concentrations in the spring of 2018 are shown in **Figure 1**. The multi-elemental characterizations of PM$_{2.5}$ aerosols successfully captured the source-specific temporal variations among elements. For example, in the middle of April (April 15–19, 2018), at a strong dust event, no large impact of anthropogenic emissions (no large enhancement of CO, BC, and sulfate) was observed by the PX-375. At the end of March (March 25–26, 2018), BC, CO, Pb, Cu, and sulfate concentrations were found to be enhanced, while whereas dust-
220   related elements such as Si and Ca showed relatively low concentrations compared to the middle of April, 2018. Furthermore, three selected periods (P1 (March 25–26, 2018), P2 (April 15–18, 2018), and P3 (April 29, 2018)) when the Japanese short-term air quality standard (AQS) for PM$_{2.5}$ was violated (daily concentration > 35 µg m^{-3}) are highlighted in this study. 5-d backward trajectories for P1, P2, and P3 are also shown in **Figure 1**. For P1 and P3, large combustion source areas (**Figure S4**) were the air mass pathways, whereas the Gobi Desert could be a possible dust source area for P2. This is consistent with
225   the observed temporal changes in the concentrations of atmospheric compositions, including anthropogenic combustion tracer

(CO and BC), dust tracer (Si), and secondary formation tracer (sulfate). During P2, Si, Ca, Mn, and Fe were abundant in the compositions of dust particles and showed the highest concentrations in the study period.

The CWTs of $PM_{2.5}$, sulfate, Pb, Cu, BC, and Fe are shown in **Figure 2**. The spatial distributions of CWTs of Pb and Cu were similar to those of BC and emissions of CO (**Figure S4**), indicating that these elements share strong emission regions with CO, where anthropogenic combustion sources dominate. On the contrary, the CWTs of Fe were found to be clearly different from them. The dust aerosols were found to be transported from the desert regions (e.g., the Gobi Desert) and be important for the large enhancement of Fe concentrations in the East Asian outflow.

3.3 Outlook on the concentrations and source apportionment of selected components simulated using the IMPACT model

The performance of the IMPACT model predicting the concentrations of selected aerosol components (BC, Fe, Si, Pb, and Cu) in $PM_{2.5}$ aerosols has already been described by Ito and Miyakawa (2023). The normalized mean biases NMB (NMB; Pearson's correlation coefficients, r) were calculated to be 52% (0.74), 11% (0.69), 10% (0.65), −14% (0.79), −51% (0.67), −15% (0.65), and −66% (0.59) for BC, Fe, Si, Pb, Cu, Ca, and Mn, respectively. This indicated that (1) the concentrations of Fe, Si, Pb, and Ca were reasonably well predicted (NMB < ±20%) as their r values were high (0.65–0.79), (2) the concentrations of Cu and Mn had large negative NMB values (NMB < −50%) with moderately high r values (0.59–0.67), and (3) the concentrations of BC were overestimated but with a high r value (> 0.7).

The tagged tracer analyses using the IMPACT model simulations suggested that the observed concentrations of BC, Pb, and Cu in Fukue Island were dominated by anthropogenic sources over the East Asian continent (concentration-weighted averages of 94%, 99%, and 93%, respectively), and Si originated from desert areas over the East Asian continent (concentration-weighted average of 92%) during the study period. Miyakawa et al. (2019) used radiocarbon and molecular marker analyses for the carbonaceous aerosols and found that fossil fuel combustion was the dominant source of BC (approximately 90%) in East Asian outflow in the spring of 2015, which is consistent with the dominant anthropogenic contribution to BC concentrations modeled in this study. Ca in $PM_{2.5}$ aerosols was also primarily affected by dust (concentration-weighted average of 71%), whereas sea sprays contributed secondarily (concentration-weighted average of 17%), which is higher than anthropogenic contributions (concentration-weighted average of 10%). It was found that natural sources were important for the observed Ca concentrations in $PM_{2.5}$ aerosols and that Si is a better tracer for dust aerosols than Ca.

In this study, the emission and transport of the anthropogenic components BC, Pb, and Cu in $PM_{2.5}$ aerosols and the source apportionment of Fe and Mn in $PM_{2.5}$ aerosols were investigated using specific tracers for the anthropogenic and dust emissions via the evaluations of the IMPACT model performances. The former, as discussed in Sect. 3.4, included the evaluations of the emission ratios of Pb and Cu with BC and CO, the wet removals of Pb and Cu, and the comparisons of the observations with the model simulations. The latter, as discussed in Sect. 3.5, included the analyses of the results of the source apportionment results in terms of the elemental composition of $PM_{2.5}$ dust aerosols and the enhancement ratios of anthropogenic Fe and Mn to BC in the springtime East Asian outflow.

3.4 Emissions and transport of anthropogenic aerosol components (BC, Pb, and Cu)

Pb, Cu, and a combustion tracer, BC, were analyzed in terms of their emission and transport in the East Asian outflow, considering the dominance~~s~~ of their anthropogenic sources based on the IMPACT model results (Sect. 3.3). Pb and Cu showed a positive correlation with BC (r^2 = 0.72 and 0.66, respectively; **Figure 3**), which is consistent with their temporal variations (**Figure 1b**). ~~Since~~ Because BC aerosol particles in the East Asian outflow are efficiently removed from the atmosphere by the ~~rainout~~ in-cloud scavenging and the subsequent precipitation~~process~~ (Kanaya et al., 2016; Miyakawa et al., 2017; Moteki et al., 2012), Pb and Cu can also be affected by the~~se~~ ~~wet depositions~~processes during transport. The correlations of Pb and Cu with CO were investigated to examine the removal of Pb and Cu relative to CO. In this study, the enhancement of CO from its background was used for this analysis because CO has a longer lifetime of approximately 2 months than a typical transport time scale from the East Asian continent to Fukue Island (approximately 2d; Kanaya et al., 2016) and does not get affected by wet deposition processes. The enhancement of CO from its background CO_{bkg} ($\Delta CO \equiv CO - CO_{bkg}$) was calculated following Kanaya et al. (2016; 2020). **Figures 3c** and **3d** depict the correlations of Pb and Cu with ΔCO, respectively, and show that Pb has a better correlation with BC and CO than Cu. This indicates that Cu possibly~~probably~~ has different emission sources from BC, Pb, and CO in East Asia, even though the similarity of their geospatial patterns was indicated by the CWTs for BC, Pb, and Cu. The datasets of Pb and Cu were classified into APT > 1 mm~~ h~~ and $\leq$ 1 mm~~ h~~ (i.e., more and less affected by the wet removal, respectively) to roughly diagnose the effects of wet removal on the transport of Pb and Cu (**Figures 3c** and **3d**). Notably, the relative enhancement of Pb to ΔCO was smaller for the APT > 1 mm~~ h~~ than for that $\leq$ 1mm~~ h~~.

To compensate for the concentration changes induced by the atmospheric dilution during the transport, the concentrations of X (X = BC, Pb, and Cu) normalized by the longer-lived species concentrations were analyzed to diagnose the transport efficiency. The enhancement ratios of component X to CO, $\Delta X/\Delta CO$, during the observation period were evaluated by selecting the data with an APT of zero (**Table 1**). The background levels for BC, Pb, and Cu were assumed to be zero (Kanaya et al., 2016; Miyakawa et al., 2017). The emission ratios of X to CO (ER_{XtoCO}) were determined by selecting the data points of $\Delta X/\Delta CO$ when ΔCO was > 20 ppb, continental air masses were transported, concentrations of Pb and Cu were higher than their LOD, and APT equals zero (i.e., no precipitation during the transport), which was basically the same as the method given by Kanaya et al. (2016). The ER_{XtoCO} values for X = BC, Pb, and Cu during the entire observation period (March, April, and May; MAM) were evaluated to be 4.75 ($\pm$1.39) ng m^{-3} ppb^{-1}, 177.8 ($\pm$88.8) pg m^{-3} ppb^{-1}, and 73.5 ($\pm$42.2) pg m^{-3} ppb^{-1}, respectively. ~~Since~~ Because no significant difference (p > 0.05) was found in the ER_{XtoCO} for BC, Pb, and Cu between April and May in 2018, they were merged into one dataset group "April–May" in 2018. The ER_{XtoCO} for Pb and Cu had relatively large and significant differences (p < 0.01) between March and April–May in 2018 compared to that for BC, indicating the seasonal variations in emission ratios of the anthropogenic sources of Pb and Cu over the East Asian continent. To the best of our knowledge, this is the first attempt to evaluate the emission ratios of Pb and Cu to CO in East Asia.

Table 1 ER_{XtoCO} in the East Asian outflow.

	ER$_{BCtoCO}$			ER$_{PbtoCO}$			ER$_{CutoCO}$		
	[ng m^{-3} ppb^{-1}]			[pg m^{-3} ppb^{-1}]			[pg m^{-3} ppb^{-1}]		
Month	Avg.	Std.	N	Avg.	Std.	N	Avg.	Std.	N
March	4.22	1.04	42	157.6	82.0	42	46.7	19.7	42
April	5.27	1.53	42	190.2	89.6	42	94.7	40.8	41
May	4.94	1.13	4	258.4	76.5	4	137.0	43.4	4
Apr–May	5.24	1.49	46	196.1	91.7	46	98.5	42.3	45
MAM*	4.75	1.39	88	177.8	88.8	88	73.5	42.2	87

*MAM indicates March, April, and May of 2018 (i.e., the entire observation period).

ER$_{XtoCO}$ values were used to calculate the transport efficiency of X (TE$_X$) as (ΔX/ΔCO)/ER$_{XtoCO}$. **Figure 4** depicts TE$_{BC}$, TE$_{Pb}$, and TE$_{Cu}$ as functions of the APT. As a reference, the long-term mean TE$_{BC}$-APT relationship (2009–2015) evaluated by Kanaya et al. (2016) was compared. While TE$_{Pb}$ showed a similar relationship with the APT to TE$_{BC}$, the decreasing trend of the TE$_{Cu}$-APT relationship was not steep, probably because Cu has characteristics of emission, size distributions, and mixing states different from BC and Pb. Previous studies atin urban cities illustrated that Cu exhibited the different size distributions from other components such as Pb (e.g., Yang et al., 2023) and BC (e.g., Fang et al., 2017). Indeed, Kinase et al. (2022) reported continuous observations of trace metals in PM$_{2.5}$ aerosols in an urban area of western Japan and showed that Cu concentrations were poorly correlated (r^2 = 0.17) with Pb concentrations when the local impact was significant and that approximately 60% of Cu-containing particles did not contain Pb as analyzed using an electron microscopic technique. BecauseSince the length of the observation periods and the number of data points were limited, the development of robust fit functions was difficult in this study. TE$_{Pb}$ decreased with an increase in APT, similar to TE$_{BC}$. Although the tendency of TE$_{Cu}$ was not as steep as that of TE$_{BC}$ and TE$_{Pb}$, its values were significantly less than unity (p < 0.01) for the data points with APT values higher than 0.5 mm h. Consequently, the concentrations of BC, Pb, and Cu in PM$_{2.5}$ aerosols can be concluded to be affected by the wet removal during transport in the East Asian outflow in the spring of 2018.

Modeled BC, Pb, and Cu concentrations were evaluated in terms of APT (**Figures 5** and **S5**). The IMPACT model reasonably predicted the concentrations of Pb and overestimated those of BC by 44% for the data with APT < 1 mm (i.e., small impact of the wet removal during the transport). For BC and Pb, the ratios of modeled to observed concentrations (M/O) with wet removal impacts were higher than those with no precipitation. This result and the observed decreasing trend of TE$_{BC}$ and TE$_{Pb}$ with increasing APT indicate that the wet removal processes for BC and Pb were weaker in the IMPACT model than in reality. The IMPACT model systematically underestimated the concentrations of Cu by 45% on average, indicating that the anthropogenic Cu emission inventory used in this study needs revision. We analyzed the observation-to-model differences for Cu in the base simulation with Cu$_{CuSmelt}$ calculated in the improved simulation (**Figure S6**). Although the correlation for 4-hourly data set is scattered (r^2 = 0.22), the bias can be mostly (at least >60% on average) accounted for by the Cu smelting sources. The large

書式を変更: 下付き
書式を変更: フォント: 太字
書式を変更: 上付き

variability in the bias-$Cu_{CuSmelt}$ correlation is likely caused by that $(Cu/Fe)_{CuSmelt}$ can be highly variable depending on the phase of processes and the types of the smelting facilities (e.g., Barcan, 2002; Skeaff et al. 2011) and size-dependent (Sorooshian et al., 2012), the latter of which showed the smaller values of $(Cu/Fe)_{CuSmelt}$ for submicron particles than supermicron particles.

320 Given the large uncertainties, the improved simulation evaluated the average contribution of $Cu_{CuSmelt}$ to total Cu as 40.5% (±5.2%). The tire or brake wear emissions from road transport (i.e., road brake, Kajino et al., 2020) are other possible causes of the underestimation, because a laboratory experiment study indicated that most brake wear Cu-containing particles existed in fine mode (i.e., $PM_{2.5}$) (Hagino et al., 2016). Therefore, more detailed characterizations of Cu emissions from non-combustion sources such as the smelting and road brake are critically needed.

325 The trend of M/O ratios against APT for Cu in the base and improved simulations showed no substantial ~~decreasing~~ increasing trend, similar to BC and Pb. This is caused by the difference in the TE-APT relationship for BC, Pb, and Cu between the observation and the model simulations (**Figure S7**). ~~The variability of M/O ratios for Cu was not controlled solely by the uncertainty in relation to the wet removal process, which is consistent with the gently decreasing trend of the TE_{Cu}-APT relationship.~~ ~~Nonetheless~~Although the APT was not a strong forcing factor of TE_{Cu}, the removal processes ~~and emissions~~ of

330 Cu were not properly simulated by the IMPACT model, as indicated by the relationship between~~correlation of~~ the M/O ratios ~~for Cu with~~ and TE_{Cu} for BC, Pb, and Cu, as shown in **Figure ~~S6~~S8**. We found that~~Both~~ the wet removal ~~efficiencies of aerosols in the IMPACT model~~ ~~emissions and transport of Cu aerosols~~ needs to be revised~~further investigation in the future~~.

3.5 Source apportionment analyses

3.5.1 Validation of multiple linear regression analysis for source apportionment

335 Based on the IMPACT model simulations, Si and BC can be used as excellent tracers for dust and anthropogenic primary emission sources, respectively; therefore, the source apportionment of Fe and Mn in $PM_{2.5}$ aerosols can be performed using these tracers. Source apportionment of $PM_{2.5}$ aerosols was conducted using the observed BC, Si, and sulfate concentrations ($[BC]_t$, $[Si]_t$, and $[SO_4^{2-}]_t$, respectively) to validate the use of these tracers for the source apportionment of Fe and Mn. ~~Since~~ Because $[BC]_t$ showed a positive correlation with $[SO_4^{2-}]_t$ ~~sulfate~~ (**Figure ~~S7~~S9**), the temporal variations of BC may not be

340 completely independent ~~from~~ of those of sulfate. However, BC showed a better correlation with an independent combustion source tracer of CO than sulfate (**Figure ~~S7~~S9**), indicating that the temporal variations of BC concentrations can account for those of both anthropogenic aerosols and a part of secondary aerosol concentrations. Additionally, sulfate concentrations can be used to constrain the secondary formation component in $PM_{2.5}$ aerosols through the aqueous phase reactions inside aerosol particles and cloud droplets, which cannot be represented by the temporal variations of BC concentrations. Consequently, it

345 can be concluded that both BC and sulfate can be used for the multiple linear regression (MLR) analysis. The validity of selecting Si, BC, and SO_4^{2-} as the input variables for the MLR models is described in Sect. S1 of the supporting information. The observed temporal variations of $PM_{2.5}$ aerosol concentrations ($[PM_{2.5}]_t$) were fitted in the following MLR model:

書式を変更: 下付き

書式を変更: 下付き

書式を変更: 下付き

書式を変更: フォント: 太字

書式を変更: 下付き

$$[PM_{2.5}]_t = g_{BC} \cdot [BC]_t + g_{Si} \cdot [Si]_t + g_{sulfate} \cdot [SO_4^{2-}]_t + C \qquad \text{(Eq. 2)}$$

350

The coefficients g_X (X = BC, Si, and sulfate) and C (i.e., constant term) were determined by the least squares method. As the coefficient of determination of the correlation between reconstructed and observed $PM_{2.5}$ concentrations was 0.85 (**Figure** ~~S9~~**S11**), this linear combination model accounts for most of the observed variances in $PM_{2.5}$ concentrations. C was evaluated to be 4.95 (±0.60) μg m^{-3}, which can correspond to the background level of $PM_{2.5}$ concentration (including sea-salt aerosols)

355 in the East Asian outflow in the spring of 2018. **Figure 6a** depicts the temporal variations of the observed and source-classified concentrations of $PM_{2.5}$ aerosols during the observation period. The concentrations and contributions of BC-, sulfate-, and dust-related aerosols in $PM_{2.5}$ aerosols for the entire and selected periods are shown in **Figure 6b**. The highest concentrations and dominant contributions of dust-related aerosols were observed during P2, which is consistent with the air mass transport presented in Sect. 3.2. An independent method, co-located Lidar measurement at the same site, was applied to validate our

360 source apportionment results for the dust contribution (**Figures 6c** and **6d**). Lidar-derived dust contribution to total extinction near the surface was positively correlated with the estimated dust contributions to total $PM_{2.5}$ (i.e., $g_{Si} \cdot [Si]_t/[PM_{2.5}]_t$) for the selected periods (P1, P2, and P3) at higher aerosol loadings during the observation periods. These considerations indicate that this approach can successfully analyze the source apportionment of $PM_{2.5}$ aerosols, especially dust and non-dust contributions, using the temporal variations of tracer compounds.

365 **3.5.2 Source apportionment of Fe and Mn**

~~Since~~ Because the estimation of the dust contribution using Si as a tracer was validated in Sect. 3.5.1, the same approach was applied to the observation-based source apportionment of Fe and Mn. The IMPACT model simulations suggested that the Fe and Mn concentrations at the observation site were affected by anthropogenic and lithogenic sources, with negligible impact from biomass burning during the spring of 2018 (Ito and Miyakawa, 2023). The Eq. (2) for the source apportionment of $PM_{2.5}$

370 was modified into the following Eq. (3):

$$[Y]_t = g_{BC,Y} \cdot [BC]_t + g_{Si,Y} \cdot [Si]_t + C_Y \qquad \text{(Eq. 3)}$$

$g_{X,Y}$ (X = BC and Si; Y = Fe and Mn), and C_Y (constant term) were determined by the least squares method. Notably, the BC-

375 related components of Fe and Mn can be regarded as their anthropogenic contributions due to the lack of secondary formation processes for Fe and Mn. C_{Fe} and C_{Mn} were almost zero in this study. As the coefficients of determination of the correlation between reconstructed and observed Fe and Mn concentrations were 0.97 and 0.92, respectively (**Figure** ~~S9~~**S11**), this linear combination model also accounts for almost all the observed variances of Fe and Mn concentrations. The anthropogenic contribution to total Fe in $PM_{2.5}$ aerosols was 17% (±11%) on average, which was similar to that simulated by the IMPACT

380 model (22±17%). Furthermore, the derived range was comparable to that (10–50%) estimated using the stable isotope ratio of Fe (δ^{56}Fe) of $PM_{2.5}$ aerosols transported from the East Asian continent to the northwestern Pacific Ocean (Kurisu et al., 2021).

The anthropogenic contribution to total Mn in $PM_{2.5}$ aerosols was 44% (±20%) on average, which was in reasonable agreement with that simulated by the IMPACT model (42±23%) and was higher than that of Fe. Variations in the anthropogenic and dust contributions to total Fe and Mn concentrations in $PM_{2.5}$ aerosols are further discussed in the following section.

385 The derived anthropogenic- and dust-Fe concentrations showed reasonable agreements with those simulated by the IMPACT model (most of the data points fell into the range of the factor of 2, **Figure** ~~S10~~**S12**). The M/O ratios for both anthropogenic- and dust-Fe with no precipitation (APT = 0) were approximately 0.7, which was lower than expected from the M/O ratios for total Fe for all the data with or without the impacts of the precipitation as indicated in Sect. 3.3. ~~Since~~ Because the deviation was approximately 30%, which can be accounted for by the observation uncertainty of Fe, Si, and BC, both anthropogenic Fe

390 and dust emissions and Fe concentration in dust aerosol particles were underestimated in the model simulations. The derived anthropogenic and dust-Mn concentrations were systematically higher than those simulated by the IMPACT model (**Figure** ~~S10~~**S12**), suggesting that both anthropogenic- and dust-Mn concentrations were underestimated by the IMPACT model. The underestimation of anthropogenic- and dust-Mn concentrations can be accounted for by the uncertainties in the anthropogenic emissions of Mn and the Mn content in dust aerosols (described in the later section) prescribed in the IMPACT model.

395 **3.5.3 Enhancement ratios of anthropogenic Fe and Mn to BC in the springtime East Asian outflow**

$g_{BC,Fe}$ represents the enhancement ratio of anthropogenic-Fe to BC and was determined to be 0.13 (±0.03) μg μg^{-1}. This value is significantly higher than the Fe/BC ratios derived from biomass burning (0.02 μg μg^{-1}) observed for fine-mode aerosols in the Amazon (Luo et al., 2008), which is consistent with the IMPACT's model prediction of a negligible influence of biomass burning on the observed Fe concentrations. ~~On the other hand~~However, the derived value here is lower than the magnetite-

400 Fe/BC ratio of 0.25 observed at the same observation site in the spring of 2020 (Yoshida et al., 2020). The contribution of magnetite-Fe to total anthropogenic Fe was evaluated to be approximately 40% (Matsui et al., 2018; Ito and Miyakawa, 2023), indicating a large difference in anthropogenic-Fe/BC ratios between this and the previous study (Yoshida et al., 2020). The possible reasons for this may be the differences in the year of the observations (2018 vs. 2020), analytical technique, and sampling condition. In the recent decade, BC emissions from China substantially decreased (Kanaya et al., 2020; 2021),

405 indicating that anthropogenic emissions of primary aerosols in China also decreased. However, if the anthropogenic-Fe emissions are not majorly reduced over time, the ratio of anthropogenic-Fe to BC might increase. Since the recent reduction of BC emissions was primarily attributed to the industrial sector and then the residential sector (Kanaya et al., 2020), the emission changes cannot account for all the differences in the ratio of anthropogenic-Fe to BC. Yoshida et al. (2020) applied the laser-induced incandescence technique to detect airborne single particles containing iron oxide in the size range of 170−

410 2100 nm of mass-equivalent diameter, whereas this study applied the XRF analysis to the bulk aerosol samples collected through the $PM_{2.5}$ cyclone. As concluding the major factor accounting for the discrepancy is difficult, integrated studies applying other independent analytical techniques are needed in the future. Chemical speciation of Fe-containing aerosols based

on X-ray absorption fine structure spectroscopy (Kurisu et al., 2019; 2021; Sakata et al., 2022; Takahashi et al., 2011) could be promising for further investigating the anthropogenic-Fe in ~~the~~ East Asian outflow.

415     $g_{BC,Mn}$ represents the enhancement ratio of anthropogenic-Mn to BC and was determined to be 17.1 ($\pm$1.1) ng μg^{-1}. To the best of our knowledge, this is the first time that the enhancement ratios of Mn to BC are evaluated from the ambient measurements of anthropogenic sources in the East Asian outflow, which can be used as a useful constraint to estimate the anthropogenic contribution to Mn in East Asian outflow regions.

3.5.4 Elemental concentrations of Si, Fe, and Mn in PM$_{2.5}$ dust aerosols

420   Based on the source apportionment results, elemental concentrations of Si, Fe, and Mn were estimated and compared with those evaluated in previous studies that analyzed Asian dust samples collected at Andong, Deokjeok Island, and Seoul in Korea (Jeong, 2020) and Yulin in China (Wang et al., 2011) and those simulated by the IMPACT model (Ito and Miyakawa, 2023) (**Figure ~~S11~~S13**). Note that these observation-based characterizations of dust elemental compositions were not significantly affected by non-dust components as expected from enrichment factor analyses (Jeong, 2020; Wang et al., 2011). g_{Si}^{-1} (=

425 $[Si]_t/(g_{Si} \cdot [Si]_t)$) can be regarded as the concentration of Si in PM$_{2.5}$ dust aerosols and was determined to be 21.6% (20.4–23.1%) in this study. This value is consistent with that given in a previous study (26.99$\pm$1.24%) that analyzed Asian dust in total suspended particulate matter (TSP) collected from Korea (Jeong, 2020). Note that 22.1% of PM$_{2.5}$ dust aerosols was prescribed for Si content in the model for comparison with the observations (Ito and Miyakawa, 2023). Although the uncertainty in the quantification of $[Si]_t$ was not evaluated prior to the observation, the derived values of g_{Si}^{-1} were reasonably comparable to the

430 other independent evaluations. On changing the $[Si]_t$ by $\pm$20%, the values of g_{Si}^{-1} were determined to be 17.3–26.0% ($-$20% to $+$20% cases), without significant changes in the fitted values of g_{BC}, $g_{sulfate}$, and C. This indicates that the source apportionment of PM$_{2.5}$ aerosol concentrations was not strongly affected by the uncertainty of $[Si]_t$, and the uncertainty of $[Si]_t$ was estimated to be not so high (~15% at most).

    $g_{Si,Fe} \cdot g_{Si}^{-1}$ (= $g_{Si,Fe} \cdot [Si]_t/(g_{Si} \cdot [Si]_t)$) represents the concentration of Fe in dust aerosols (7.3$\pm$0.5%), which was evaluated in Korea

435 (5.27$\pm$0.25%) and China (3.98% of PM$_{2.5}$ aerosols collected at Yulin, China) and was compared with that simulated by the IMPACT model (3.83$\pm$0.26% at the observation site). $g_{Si,Mn} \cdot g_{Si}^{-1}$ (= $g_{Si,Mn} \cdot [Si]_t/(g_{Si} \cdot [Si]_t)$) represents the concentration of Mn in dust aerosols (0.21$\pm$0.01%), which was evaluated to be 0.12$\pm$0.01% by Jeong (2020) and 0.11% by Wang et al. (2011). Note that 0.077% of PM$_{2.5}$ dust aerosols was prescribed for Mn content in the model for comparison with the observations (Ito and Miyakawa, 2023). The concentrations of Fe and Mn in PM$_{2.5}$ dust aerosols estimated in this study were higher than those given

440 in the independent evaluations. However, the orders of the evaluated elemental concentrations of all the selected elements (Si, Fe, and Mn) were the same as in all the independent evaluations. On changing $[Si]_t$ by $\pm$20%, the derived values of $g_{Si,Fe} \cdot g_{Si}^{-1}$ and $g_{Si,Mn} \cdot g_{Si}^{-1}$ would not change without the significant changes in the determinations of $g_{BC,Fe}$, $g_{BC,Mn}$, C_{Fe}, and C_{Mn}, because the increases (decreases) in $g_{Si,Fe}$ and $g_{Si,Mn}$ were almost completely compensated by decreasing (increasing) $[Si]_t$. This indicates that the source apportionment of Fe and Mn aerosol concentrations and their elemental mass concentrations in dust aerosols

445 were not significantly affected by the uncertainty of $[Si]_t$. The uncertainty of $[BC]_t$ (22%) also did not affect the calculations

of the fitting coefficients in the MLR model. The possible causes of higher Fe and Mn concentrations may be the contributions of anthropogenic Si-containing particles with higher Fe and Mn contents, such as fly ash (e.g., Li et al., 2012; Liu et al., 2019), and the contributions of "anthropogenic" dust sources associated with the agricultural land use change (~40% in East Asia, e.g., Ginoux et al., 2012). Due to limited knowledge of the difference in dust elemental composition between natural and anthropogenic sources, further investigations of the elemental compositions of both natural and anthropogenic dust aerosol particles are needed in the future. Note that the discrepancies can also be partly accounted for by the uncertainties in measuring $[Fe]_t$ and $[Mn]_t$ (26% and 23%, respectively) using the PX-375.

3.5.5 Variations in the anthropogenic contribution of total Fe and Mn in PM$_{2.5}$ aerosols

Figure 7 depicts the temporal variations of the observed and source-classified concentrations of Fe and Mn during the observation period. During P2 (the strong dust period), both elements showed the highest concentrations in the entire observation period. The estimated dust Fe and Mn also showed the highest concentrations in the entire observation period. The anthropogenic sources contributed to 2.1% (±1.2%) and 8.8% (±4.3%) of total Fe and Mn, respectively, in PM$_{2.5}$ aerosols during P2. During P1 and P3, the anthropogenic contributions increased by approximately 30% and 65% of total Fe and Mn, respectively, in PM$_{2.5}$ aerosols. It was found that depending on the air mass origin, the anthropogenic or dust contributions to the observed Fe and Mn concentrations greatly varied, and the anthropogenic contributions to total Fe and Mn were inversely proportional to the total concentrations of Fe and Mn in the spring of 2018 (**Figure 8**). ~~Since~~ Because Asian dust aerosols are frequently transported from the desert region (e.g., the Gobi Desert) over the East Asian continent towards the outflow area, such as the Pacific Ocean, in the spring season (e.g., Wan et al., 2020), the large springtime enhancements in the concentrations of Fe and Mn in the East Asian outflow are substantially affected by the dust emissions over the East Asian continent.

In the East Asian outflow, the fractional solubilities of combustion-derived and dust-derived Fe were estimated to be 11% and 0.9%, respectively (Kurisu et al., 2021). Assuming applying these fractional water solubilities (f_{sol}) of Fe to our data, the estimated water-soluble Fe concentration (17.7 ng m^{-3}) during P1 and P3 (the periods with fewer impacts of dust) was comparable to 19.0 ng m^{-3} during P2 (the dust-dominated period), even though the total Fe concentrations during P1 and P3 were almost 30% of that during P2. ~~Since~~ Because the f_{sol} of Fe can be affected by atmospheric processing during transport and can be as high as ~50% for fine mode aerosols over the remote ocean (Sholkovitz et al., 2012 and references therein), the evaluations of water-soluble Fe contributions during P1 and P3 might be substantially underestimated. These considerations supported the importance of anthropogenic sources that deliver water-soluble Fe to the East Asian outflow region, as suggested in previous studies (e.g., Ito and Miyakawa, 2023). The f_{sol} of Mn is typically higher than that of Fe and does not exhibit the same large variabilities in f_{sol} as Fe (Baker et al., 2013; 2014; Shelley et al., 2018). The enhancements of Mn concentrations originating from both anthropogenic and dust sources can lead to substantial impacts of the water-soluble fraction of Mn on adverse health effects (i.e., ROS production) in the East Asian outflow region (e.g., Nishita-Hara et al., 2019) and ocean biogeochemistry as a micronutrient to limit or co-limit microbial activities (e.g., Ahlgren et al., 2014; Moore et al., 2013).

Further characterizations of the f_{sol} of Mn are critically needed to elucidate their variabilities and differences between anthropogenic and dust sources.

480 **4 Conclusions**

In this study, semi-continuous measurements of the elemental composition of fine mode (PM$_{2.5}$) aerosols were conducted on Fukue Island in western Japan during the spring of 2018. An automated X-ray fluorescenceRF analyzer, PX-375, was successfully deployed, which has the capability to measure the aerosol's elemental compositions with a temporal resolution of a few hours even in remote regions after long-range transport from emission source regions. Four Four-hourly mass
485 concentrations of climatologically and geochemically important elements, such as S, Pb, Cu, Si, Ca, Fe, and Mn, in PM$_{2.5}$ aerosols were reported during the observation period. Furthermore, measurements of other atmospheric compositions, such as BC and CO, were conducted to analyze the emission and transport from the combustion sources over the East Asian continent. Positive correlations of Pb and Cu with BC and CO and the similarity of their CWTs indicatedwere found during the observation period, which indicate that the emission sources of these metals share the region where the large CO (and BC)
490 emission sources are located. The use of CO, which is physicochemically stable on the time scale of atmospheric transport of aerosol particles, enabled us, for the first time, to successfully analyze the emissions of Pb and Cu and the impacts of the wet removal during the transport on their concentrations through the observations at the receptor site. The continental outflow air masses with minimized impacts of the wet removal during the transport were extracted to elucidate the emission ratio of Pb and Cu to CO, which were evaluated for the spring of 2018 in the East Asian outflow to be 152.7 and 63.1 µg g^{-1}, respectively.
495 With increasing APT, the transport efficiency of Pb was found to decrease similar to that of BC, suggesting that the wet removal rates of Pb were almost the same as those of BC during the springtime East Asian outflow. Notably, Cu possessed a nature different from BC and Pb in terms of emission sources and wet removal in the East Asian outflow. Further simultaneous time-series characterizations of suchsize-resolved elemental concentrations and mixing states are highly desirable to elucidate the mechanisms controlling their wet removal rates. The source apportionment of these elements was evaluated by comparing
500 the simulations obtained from the IMPACT model with those observed by the PX-375 and was verified in terms of the emission and wet removal processes. From the analysis of the tagged tracer simulations by the IMPACT model, BC and Si could be used as tracers for anthropogenic and dust emissions, respectively, during the observation period. The source apportionments of Fe and Mn in PM$_{2.5}$ aerosols were found based on MLR analysis that used observed Si and BC tracers, and revealed that the anthropogenic contribution to total Fe and Mn in PM$_{2.5}$ aerosols was 17% and 44%, respectively, on average in the spring
505 of 2018, corresponding to the range of 2%–29% and 9%–68% during the high PM$_{2.5}$ concentration periods depending on their air mass origins. However, the anthropogenic contributions of Fe were not dominant; the variations of anthropogenic Fe can regulate adverse health effects and ocean biogeochemistry due to its higher water solubility. The modeled BC, Pb, Cu, and Fe were evaluated by separately considering their emission and transport. Ratios of modeled to observed concentrations for these components were analyzed in terms of the APT from the East Asian continent. This indicated that the current model simulations

510 overestimated the CEDS (v2021-02-05)-based emissions of BC by 44% and underestimated Cu by 45%, anthropogenic Fe by 28% in East Asia, and the wet deposition rates for BC and Pb. The Cu smelting sources can account for most of the model underestimation of Cu emissions. This study provides insights into the importance of removal process investigations, source apportionment of Fe, and high-temporal resolution measurements of aerosol trace elemental compositions.

Data availability

515 All the observation and model simulation data used in this study, except the lidar observation data sets, will be available online (https://doi.org/10.5281/zenodo.8385331, Miyakawa et al., 2023)at a data repository such as Zenodo and PANGAEA. The lidar observation data sets are available at the website of AD-Net, hosted by the National Institute for Environmental Studies, Japan (https://www-lidar.nies.go.jp/AD-Net/).

Author contribution

520 **Conceptualization:** T. M.; **Data curation:** T. M., A. I., A. S.; **Formal analysis:** T. M.; **Funding acquisition:** A. I., T. M.; **Investigation:** All authors; **Methodology:** T. M., A. I.; **Writing – original draft preparation:** T. M.; **Writing – review & editing:** All authors

Competing interests

Y. K. is an editorial board member of *Atmospheric Chemistry and Physics*. Y. M. and E. M. are employees of Horiba Ltd.,
525 which developed the continuous particulate monitor with the X-ray fluorescence analysis (PX-375) used in this study.

Acknowledgements

This study was supported by the JSPS KAKENHI (Grant No.: JP20H04329), MEXT-Program for the Advanced Studies of Climate Change Projection (SENTAN) (Grant No.: JPMXD0722681344), Environmental Research and Technology Development Fund (Grant no.: JPMEERF20222001) of the Environmental Restoration and Conservation Agency provided by
530 Ministry of the Environment of Japan, and Steel Foundation for Environmental Protection Technology (Grant No.: C-48-12). We acknowledge M. Kubo, T. Takamura, and H. Irie (Chiba University) for their support at the Fukue Island's Atmospheric Environment Monitoring Station. Numerical simulations were performed using the Earth Simulator 4 at the Japan Agency for Marine-Earth Science and Technology. We thank two anonymous reviewers for their constructive comments. We would like to thank Editage (https://www.editage.com/) for English language editing.

535 **References**

Asano, H., Aoyama, T., Mizuno, Y., Shiraishi, Y.: Highly time-resolved atmospheric observations using a continuous fine particulate matter and element monitor. ACS Ear. Spa. Chem., 1(9), 580–590, https://doi.org/10.1021/acsearthspacechem.7b00090, 2017.

Ahlgren, Nathan A., Noble, Abigail, Patton, Allison P., Roache-Johnson, Kathryn, Jackson, Laurel, Robinson, Daniela, McKay, 540 Cedar, Moore, Lisa R., Saito, Mak A., Rocap, Gabrielle: The unique trace metal and mixed layer conditions of the Costa Rica upwelling dome support a distinct and dense community of Synechococcus, Lim. Ocea., 59, https://doi.org/10.4319/lo.2014.59.6.2166, 2014.

Baker, A. R., Adams, C., Bell, T. G., Jickells, T. D. and Ganzeveld L. : Estimation of atmospheric nutrient inputs to the Atlantic Ocean from 50°N to 50°S based on large-scale field sampling: iron and other dust-associated elements. Glo. Biog.. Cyc., 545 27, 755–767, https://doi.org/10.1002/gbc.20062, 2013.

Baker, A., Laskina, O. and Grassian, V.: in Mineral Dust: A Key player in the Earth System (eds Knippertz, P. & Stutt, J.-B) 75-92 (Springer Science+Business Media, Dordrecht), 2014.

Barcan, V.: Nature and origin of multicomponent aerial emissions of the copper-nickel smelter complex. Environ. int., 28(6), 451–456, 2002.

550 Charrier, J. G. and Anastasio, C.: On dithiothreitol (DTT) as a measure of oxidative potential for ambient particles: evidence for the importance of soluble transition metals, Atmos. Chem. Phys., 12, 9321–9333, https://doi.org/10.5194/acp-12-9321-2012, 2012.

Chatani, S., Itahashi, S., and Yamaji, K.: Advantages of continuous monitoring of hourly PM2.5 component concentrations in Japan for model validation and source sensitivity analyses. Asi. J. Atmos. Environ., 15(2), 1-29, 555 https://doi.org/10.5572/ajae.2021.008, 2021.

Choi, Y., Kanaya, Y., Takigawa, M., Zhu, C., Park, S.-M., Matsuki, A., Sadanaga, Y., Kim, S.-W., Pan, X., and Pisso, I.: Investigation of the wet removal rate of black carbon in East Asia: validation of a below- and in-cloud wet removal scheme in FLEXible PARTicle (FLEXPART) model v10.4, Atmos. Chem. Phys., 20, 13655–13670, https://doi.org/10.5194/acp-20-13655-2020, 2020.

560 Draxler, R.R., Rolph, G.D.: HYSPLIT (HYbrid Single-Particle Lagrangian Integrated Trajectory) Model Access via NOAA ARL READY Website. NOAA Air Resources Laboratory, Silver Spring, Md. http://ready.arl.noaa.gov/HYSPLIT.php, 2012.

Fang, T., Guo, H., Verma, V., Peltier, R. E., and Weber, R. J.: $PM_{2.5}$ water-soluble elements in the southeastern United States: automated analytical method development, spatiotemporal distributions, source apportionment, and implications for heath 565 studies, Atm. Chem. Phys., 15, 11667–11682, https://doi.org/10.5194/acp-15-11667-2015, 2015.

Fang, T., Guo, H., Zeng, L., Verma, V., Nenes, A., and Weber, R. J.: Highly Acidic Ambient Particles, Soluble Metals, and Oxidative Potential: A Link between Sulfate and Aerosol Toxicity. Environ. Sci. Technol., 51(5), 2611–2620, https://doi.org/10.1021/acs.est.6b06151, 2017.

Ginoux, P., Prospero, J. M., Gill, T. E., Hsu, N. C., and Zhao, M.: Global-scale attribution of anthropogenic and natural dust sources and their emission rates based on MODIS Deep Blue aerosol products, Rev. Geophy., 50, RG3005, https://doi.org/10.1029/2012RG000388, 2012.

Hagino, H., Oyama, M., and Sasaki, S.: Laboratory testing of airborne brake wear particle emissions using a dynamometer system under urban city driving cycles. Atmos. environ., 131, 269-278, https://doi.org/10.1016/j.atmosenv.2016.02.014, 2016.

Hoesly, R. M., Smith, S. J., Feng, L., Klimont, Z., Janssens-Maenhout, G., Pitkanen, T., Seibert, J. J., Vu, L., Andres, R. J., Bolt, R. M., Bond, T. C., Dawidowski, L., Kholod, N., Kurokawa, J.-I., Li, M., Liu, L., Lu, Z., Moura, M. C. P., O'Rourke, P. R., and Zhang, Q.: Historical (1750–2014) anthropogenic emissions of reactive gases and aerosols from the Community Emissions Data System (CEDS), Geosci. Mod. Dev., 11, 369–408, https://doi.org/10.5194/gmd-11-369-2018, 2018.

Ichoku, C., and Ellison, L.: Global top-down smoke-aerosol emissions estimation using satellite fire radiative power measurements. Atm. Chem. Phys. 14, 6643–6667. https://doi.org/10.5194/acp-14-6643-2014, 2014.

Ito, A. and Feng, Y.: Role of dust alkalinity in acid mobilization of iron. Atmos. Chem. Phys., 10, 9237–9250, https://doi.org/10.5194/acp-10-9237-2010, 2010.

Ito, A. and Xu, L.: Response of acid mobilization of iron-containing mineral dust to improvement of air quality projected in the future. Atmos. Chem. Phys., 14, 3441–3459, https://doi.org/10.5194/acp-14-3441-2014, 2014.

Ito, A., and Kok, J. F.: Do dust emissions from sparsely vegetated regions dominate atmospheric iron supply to the Southern Ocean?. J. Geophys. Res. Atmos., 122, 3987–4002, https://doi.org/10.1002/2016JD025939, 2017.

Ito, A., Lin, G. and Penner, J.E.: Radiative forcing by light-absorbing aerosols of pyrogenetic iron oxides. Sci. Rep., 8, 7347. https://doi.org/10.1038/s41598-018-25756-3, 2018.

Ito, A., Myriokefalitakis, S., Kanakidou, M., Mahowald, N. M., Scanza, R.A., Hamilton, D.S., Baker, A.R., Jickells, T., Sarin, M., Bikkina, S. and Gao, Y.: Pyrogenic iron: The missing link to high iron solubility in aerosols. Sci. Adv., 5(5), eaau7671, 2019.

Ito, A., Ye, Y., Baldo, C. and Shi, Z.: Ocean fertilization by pyrogenic aerosol iron. Npj Clim. Atmos. Sci. 4, 30. https://doi.org/10.1038/s41612-021-00185-8, 2021.

Ito, A., and T. Miyakawa: Aerosol Iron from Metal Production as a Secondary Source of Bioaccessible Iron. Environ. Sci. Tech., 57(10), 4091–4100, https://doi.org/10.1021/acs.est.2c06472, 2023.

Ito, A., Y. Miyazaki, F. Taketani, Y. Iwamoto, and Y. Kanaya: Marine aerosol feedback on biogeochemical cycles and the climate in the Anthropocene: lessons learned from the Pacific Ocean. Environ. Sci.: Atmos., https://doi.org/10.1039/D2EA00156J, 2023.

Jeong, G. Y.: Mineralogy and geochemistry of Asian dust: dependence on migration path, fractionation, and reactions with polluted air, Atm. Chem. Phys., 20, 7411–7428, https://doi.org/10.5194/acp-20-7411-2020, 2020.

Jordi, A., Basterretxea, G., Tovar-Sanchez, A., Alastuey, A., and Querol, X.: Copper aerosols inhibit phytoplankton growth in the Mediterranean Sea. Proc. Nat. Aca. Sci., 109(52), 21246–21249, https://doi.org/10.1073/pnas.1207567110, 2012, 2012.

Kabashnikov, V. P., Chaikovsky, A. P., Kucsera, T. L., and Metelskaya, N. S.: Estimated accuracy of three common trajectory statistical methods. Atmos. Environ., 45(31), 5425–5430, https://doi.org/10.1016/j.atmosenv.2011.07.006, 2011.

Kajino, M., Hagino, H., Fujitani, Y., Morikawa, T., Fukui, T., Onishi, K., Okuda, T., Kajikawa, T. and Igarashi, Y.: Modeling transition metals in East Asia and Japan and its emission sources. GeoHeath, 4, e2020GH000259. https://doi.org/10.1029/2020GH000259, 2020.

Kajino, M., Hagino, H., Fujitani, Y., Morikawa, T., Fukui, T., Onishi, K., Okuda, T. and Igarashi, Y.: Simulation of the transition metal-based cumulative oxidative potential in East Asia and its emission sources in Japan. Sci. Rep., 11, 6550. https://doi.org/10.1038/s41598-021-85894-z, 2021.

Kanaya, Y., Pan, X., Miyakawa, T., Komazaki, Y., Taketani, F., Uno, I., and Kondo, Y.: Long-term observations of black carbon mass concentrations at Fukue Island, western Japan, during 2009–2015: constraining wet removal rates and emission strengths from East Asia, Atmos. Chem. Phys., 16, 10689–10705, https://doi.org/10.5194/acp-16-10689-2016, 2016.

Kanaya, Y., K. Yamaji, T. Miyakawa, F. Taketani, C. Zhu, Y. Choi, Y. Komazaki, K. Ikeda, Y. Kondo, and Z. Klimont: Rapid reduction of black carbon emissions from China based on 2009–2019 observations from Fukue Island, Japan, Atmos. Chem. Phys., 20, 6339–6356, https://doi.org/10.5194/acp-20-6339-202, 2020.

Kanaya, Y., K. Yamaji, T. Miyakawa, Taketani, F., Zhu, C., Choi, Y., Ikeda, K., Tanimoto, H., Yamada, D., Narita, D. and Kondo, Y.: Dominance of the residential sector in Chinese black carbon emissions as identified from downwind atmospheric observations during the COVID-19 pandemic, Sci. Rep., 11, 23378, https://doi.org/10.1038/s41598-021-02518-2, 2021.

Kinase, T., Adachi, K., Hayashi, M., Hara, K., Nishiguchi, K., and Kajino, M.: Characterization of aerosol particles containing trace elements (Ga, As, Rb, Mo, Cd, Cs, Tl, and others) and their atmospheric concentrations with a high temporal resolution. Atmos. Environ., 290, 119360, https://doi.org/10.1016/j.atmosenv.2022.119360, 2022.

Kurisu, M., Sakata, K., Uematsu, M., Ito, A., and Takahashi, Y.: Contribution of combustion Fe in marine aerosols over the northwestern Pacific estimated by Fe stable isotope ratios, Atmos. Chem. Phys., 21, 16027–16050, https://doi.org/10.5194/acp21-16027-2021, 2021.

Lakey, P. S. J., Berkemeier, T., Tong, H., Arangio, A.M., Lucas, K., Pöschl, U. and Shiraiwa, M.: Chemical exposure-response relationship between air pollutants and reactive oxygen species in the human respiratory tract. Sci. Rep. 6, 32916; https://doi.org/10.1038/srep32916, 2016.

Lamb, K.D., Matsui, H., Katich, J.M., Perring, A.E., Spackman, J.R., Weinzierl, B., Dollner, M. and Schwarz, J.P.: Global-scale constraints on light-absorbing anthropogenic iron oxide aerosols. Npj Clim. Atmos. Sci 4, 15. https://doi.org/10.1038/s41612-021-00171-0, 2021.

Li, W., Z. Shi, D. Zhang, X. Zhang, P. Li, Q. Feng, Q. Yuan, and W. Wang: Haze particles over a coal-burningregion in the China Loess Plateau in winter: Three flight missions in December 2010, J. Geophys. Res.,117, D12306, https://doi.org/10.1029/2012JD017720, 2012.

Liu, H., Yan, Y., Chang, H., Chen, H., Liang, L., Liu, X., Qiang, X., and Sun, Y.: Magnetic signatures of natural and anthropogenic sources of urban dust aerosol, Atmos. Chem. Phys., 19, 731–745, https://doi.org/10.5194/acp-19-731-2019, 2019.

Liu, L., Li, W., Lin, Q., Wang, Y., Zhang, J., Zhu, Y., Yuan, Q., Zhou, S., Zhang, D., Baldo, C. and Shi, Z.: Size-dependent aerosol iron solubility in an urban atmosphere. Npj Clim. Atmos. Sci., 5, 53. https://doi.org/10.1038/s41612-022-00277-z, 2022.

Mahowald, N.M., Hamilton, D.S., Mackey, K.R, Moore, J.K., Baker, A.R., Scanza, R.A. and Zhang, Y.: Aerosol trace metal leaching and impacts on marine microorganisms. Nat. Commun. 9, 2614. https://doi.org/10.1038/s41467-018-04970-7, 2018.

Matsui, H., Mahowald, N., Moteki, N., Hamilton, D., Ohata, S., Yoshida, A., Koike, M., Scanza, R., and Flanner, M.: Anthropogenic combustion iron as a complex climate forcer. Nature Communications, 9(1), 1593. https://doi.org/10.1038/s41467-018-03997-0, 2018.

Miyakawa, T., Oshima, N., Taketani, F., Komazaki, Y., Yoshino, A., Takami, A., Kondo, Y., and Kanaya, Y.: Alteration of the size distributions and mixing states of black carbon through transport in the boundary layer in east Asia, Atmos. Chem. Phys., 17, 5851–5864, https://doi.org/10.5194/acp-17-5851-2017, 2017.

Miyakawa, T., Y. Komazaki, C. Zhu, F. Taketani, X. Pan, Z. Wang, and Y. Kanaya: Characterization of carbonaceous aerosols in Asian outflow in the spring of 2015: importance of non-fossil fuel sources, Atmos. Environ., 214, 116858, https://doi.org/10.1016/j.atmosenv.2019.116858, 2019.

Miyakawa, T., Ito, A., Zhu, C., and Kanaya, Y.: Observed and modeled aerosol compositions at Fukue island in the spring of 2018. (Version 1) [Dataset]. ZENODO. https://doi.org/10.5281/zenodo.8385331, 2023.

Moore, C., Mills, M., Arrigo, K.R., Berman-Frank, I., Bopp, L., Boyd, P.W., Galbraith, E.D., Geider, R.J., Guieu, C., Jaccard, S.L. and Jickells, T.D.: Processes and patterns of oceanic nutrient limitation. Nature Geosci 6, 701–710. https://doi.org/10.1038/ngeo1765, 2013.

Moteki, N., Kondo, Y., Oshima, N., Takegawa, N., Koike, M., Kita, K., Matsui, H., and Kajino, M.: Size dependence of wet removal of black carbon aerosols during transport from the boundary layer to the free troposphere, Geophys. Res. Lett., 39, L13802, https://doi.org/10.1029/2012GL052034, 2012.

Myhre, G., Myhre, C. E.L., Samset, B. H. and Storelvmo, T.: Aerosols and their Relation to Global Climate and Climate Sensitivity. Nature Education Knowledge 4(5):7, 2013.

665 Nishita-Hara, C., Hirabayashi, M., Hara, K., Yamazaki, A., and Hayashi, M.: Dithiothreitol-measured oxidative potential of size-segregated particulate matter in Fukuoka, Japan: Effects of Asian dust events. GeoHealth, 3, 160–173. https://doi.org/10.1029/2019GH000189, 2019.

O'Rourke, P. R., Smith, S. J., Mott, A., Ahsan, H., McDuffie, E. E., Crippa, M., Klimont, S., McDonald, B., Wang, Z., Nicholson, M. B., Feng, L., and Hoesly, R. M.: CEDS v-2021-02-05 Emission Data 1975–2019; Zenodo,
670 https://doi.org/10.5281/zenodo.4509372, 2021.

Pacyna, J.M. and Pacyna, E.G.: An Assessment of Global and Regional Emissions of Trace Metals to the Atmosphere from Anthropogenic Sources Worldwide. Environmental Research, 9, 269–298, 2001.

Pope, C. A. and Dockery, D. W.: Health effects of fine particulate air pollution: Lines that connect, J. Air Waste Manag. Assoc., 56(6), 709–742, https://doi.org/10.1080/10473289.2006.10464485, 2006.

675 Rathod, S. D., Hamilton, D. S., Mahowald, N. M., Klimont, Z., Corbett, J. J., and Bond, T. C.: A mineralogy-based anthropogenic combustion-iron emission inventory. J. Geophys. Res.: Atmospheres, 125, e2019JD032114. https://doi.org/10.1029/2019JD032114, 2020.

Reff, A., Bhave, P. V., Simon, H., Pace, T. G., Pouliot, G. A., Mobley, J. D., and Houyoux, M.: Emissions inventory of $PM_{2.5}$ trace elements across the United States. Environ. Sci. Technol., 43, 5790–5796, https://doi.org/10.1021/es802930x, 2009.

680 Sakata, K., Kurisu, M., Takeichi, Y., Sakaguchi, A., Tanimoto, H., Tamenori, Y., Matsuki, A., and Takahashi, Y.: Iron (Fe) speciation in size-fractionated aerosol particles in the Pacific Ocean: The role of organic complexation of Fe with humic-like substances in controlling Fe solubility, Atmos. Chem. Phys., 22, 9461–9482, https://doi.org/10.5194/acp-22-9461-2022, 2022.

Shelley, R. U., Landing, W. M., Ussher, S. J., Planquette, H., and Sarthou, G.: Regional trends in the fractional solubility of
685 Fe and other metals from North Atlantic aerosols (GEOTRACES cruises GA01 and GA03) following a two-stage leach, Biogeo., 15, 2271–2288, https://doi.org/10.5194/bg-15-2271-2018, 2018.

Shimizu, A., N. Sugimoto, I. Matsui, K. Arao, I. Uno, T. Murayama, N. Kagawa, K. Aoki, A. Uchiyama, and A. Yamazaki: Continuous observations of Asian dust and other aerosols by polarization lidar in China and Japan during ACE-Asia, J. Geophys. Res., 109, D19S17, https://doi.org/10.1029/2002JD003253, 2004.

690 Shimizu, A., Sugimoto, N., Matsui, I., and Nishizawa, T.: Direct comparison of extinction coefficients derived from Mie-scattering lidar and number concentrations of particles, subjective weather report in Japan. J. Quant. Spec. Rad. Tran., 153, 77-87, https://doi.org/10.1016/j.jqsrt.2014.12.005, 2015.

Sholkovitz, E.R., Sedwick, P.N., Church, T.M., Baker, A.R., and Powell, C.F.: Fractional solubility of aerosol iron: Synthesis of a global-scale dataset, Geochim. Cosmochim. Ac, 89, 173–189, https://doi.org/10.1016/j.gca.2012.04.022, 2012.

695 Skeaff, J. M., Thibault, Y. and Hardy, D. J.: A new method for the characterisation and quantitative speciation of base metal smelter stack particulates. Environ. Monit. Assess., 177, 165–192, https://doi.org/10.1007/s10661-010-1627-9, 2011.

Sorooshian, A., Csavina, J., Shingler, T., Dey, S., Brechtel, F. J., Saez, A. E., and Betterton, E. A.: Hygroscopic and Chemical Properties of Aerosols Collected near a Copper Smelter: Implications for Public and Environmental Health. Environ. Sci. Technol., 46(17), 9473–9480, https://doi.org/10.1021/es302275k, 2012.

700 Stein, A.F., Draxler, R.R., Rolph, G.D., Stunder, B.J.B., Cohen, M.D., and Ngan, F.: NOAA's HYSPLIT atmospheric transport and dispersion modeling system. Bull. Am. Meteorol. Soc. 96, 2059–2077. https://doi.org/10.1175/BAMS-D-14-00110.1, 2015.

Sugimoto, N., Uno, I., Nishikawa, M., Shimizu, M., Matsui, I., Dong, X., Chen, Y., and Quan, H.: Record Heavy Asian Dust in Beijing in 2002: Observations and Model Analysis of Recent Events, Geophys. Res. Lett. 30, 12, 1640, 705 https://doi.org/10.1029/2002GL016349, 2003.

Szopa, S., Naik, V., Adhikary, B., Artaxo, P., Berntsen, T., Collins, W.D., Fuzzi, S., Gallardo, L. Kiendler-Scharr, A., Klimont, Z., Liao, H., Unger, N., and Zanis, P.: Short-Lived Climate Forcers. In Climate Change 2021: The Physical Science Basis. Contribution of Working Group I to the Sixth Assessment Report of the Intergovernmental Panel on Climate Change [Masson-Delmotte, V., P. Zhai, A. Pirani, S.L. Connors, C. Pean, S. Berger, N. Caud, Y. Chen, L. Goldfarb, M.I. Gomis, 710 M. Huang, K. Leitzell, E. Lonnoy, J.B.R. Matthews, T.K. Maycock, T. Waterfield, O. Yelekci, R. Yu, and B. Zhou (eds.)]. Cambridge University Press, Cambridge, United Kingdom and New York, NY, USA, pp. 817−922, https://doi.org/10.1017/9781009157896.008, 2021.

Takahashi, Y., Higashi, M., Furukawa, T., and Mitsunobu, S.: Change of iron species and iron solubility in Asian dust during the long-range transport from western China to Japan, Atm. Chem. Phys., 11, 11237–11252, https://doi.org/10.5194/acp-715 11870 875 880 11237-2011, 2011.

Tagliabue, A., Bowie, A., Boyd, P.W., Buck, K.N., Johnson, K.S., and Saito, M.A.: The integral role of iron in ocean biogeochemistry. Nature, 543, 51–59. https://doi.org/10.1038/nature21058, 2017.

Verma, R. L., Kondo, Y., Oshima, N., Matsui, H., Kita, K., Sahu, L. K., Kato, S., Kajii, Y., Takami, A., and Miyakawa, T.: Seasonal variations of the transport of black carbon and carbon monoxide from the Asian continent to the western Pacific 720 in the boundary layer, J. Geophys. Res., 116, D21307, https://doi.org/10.1029/2011JD015830, 2011.

Wan, S., Sun, Y., and Nagashima, K.: Asian dust from land to sea: Processes, history, and effect from modern observation to geological records. Geol. Mag., 157(5), 701–706. https://doi.org/10.1017/S0016756820000333, 2020.

Wang, Q., Zhuang, G., Li, J., Huang, K., Zhang, R., Jiang, Y., Lin, Y., and Fu, J. S.: Mixing of dust with pollution on the transport path of Asian dust – revealed from the aerosol over Yulin, the north edge of Loess Plateau. Sci. Tot. Environ., 725 409(3), 573–581, https://doi.org/10.1016/j.scitotenv.2010.10.032, 2011.

Yang T, Chen Y, Zhou S, and Li H.: Impacts of aerosol copper on marine phytoplankton: A Review. Atmos., 10(7):414. https://doi.org/10.3390/atmos10070414, 2019.

Yang, J., Ma, L., He, X., Au, W. C., Miao, Y., Wang, W.-X., and Nah, T.: Measurement report: Abundance and fractional solubilities of aerosol metals in urban Hong Kong - insights into factors that control aerosol metal dissolution in an urban 730 site in South China. Atmos. Chem. Phys., 23, 1403–1419, https://doi.org/10.5194/acp-23-1403-2023, 2023.

Yoshida, A., Moteki, N., Ohata, S., Mori, T., Koike, M., Kondo, Y., Matsui, H., Oshima, N., Takami, A., and Kita, K.: Abundances and microphysical properties of light-absorbing iron oxide and black carbon aerosols over East Asia and the Arctic. J. Geophy. Res.: Atmos., 125, e2019JD032301. https://doi.org/10.1029/2019JD032301, 2020.

Zhu, C., Miyakawa, T., Irie, H., Choi, Y., Taketani, F., and Kanaya, Y.: Light-absorption properties of brown carbon aerosols in the Asian outflow: Implications of a combination of filter and ground remote-sensing observations at Fukue Island, Japan, Sci. Tot. Environ., 797, 149155, https://doi.org/10.1016/j.scitotenv.2021.149155, 2021.

735
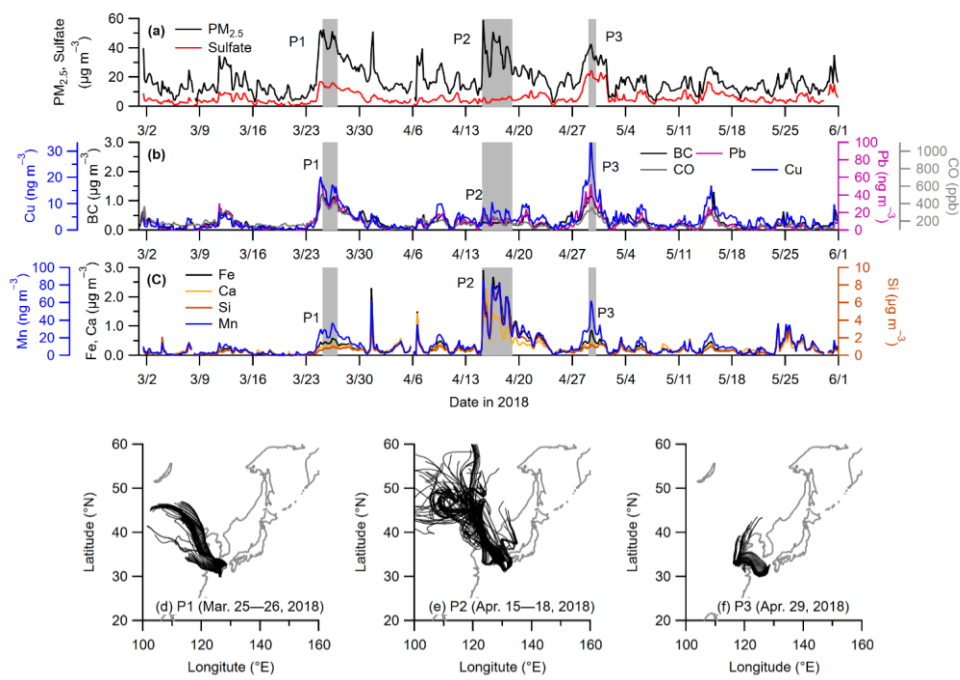
Figure 1. Temporal variations of concentrations of (a) PM$_{2.5}$ (black) and sulfate (red), (b) black carbon (BC) (black), Pb (magenta), Cu (blue), and carbon monoxide (CO) (gray), (c) Si (brown), Ca (orange), and Fe (black). The selected periods when the Japanese short-term AQS for PM$_{2.5}$ was violated (daily PM$_{2.5}$ >35 μg m^{-3}) are highlighted by the shaded areas. (d, e, and f) 5-d backward trajectories for the selected periods P1 (March 25–26, 2018), P2 (April 15–18, 2018), and P3 (April 29, 2018).
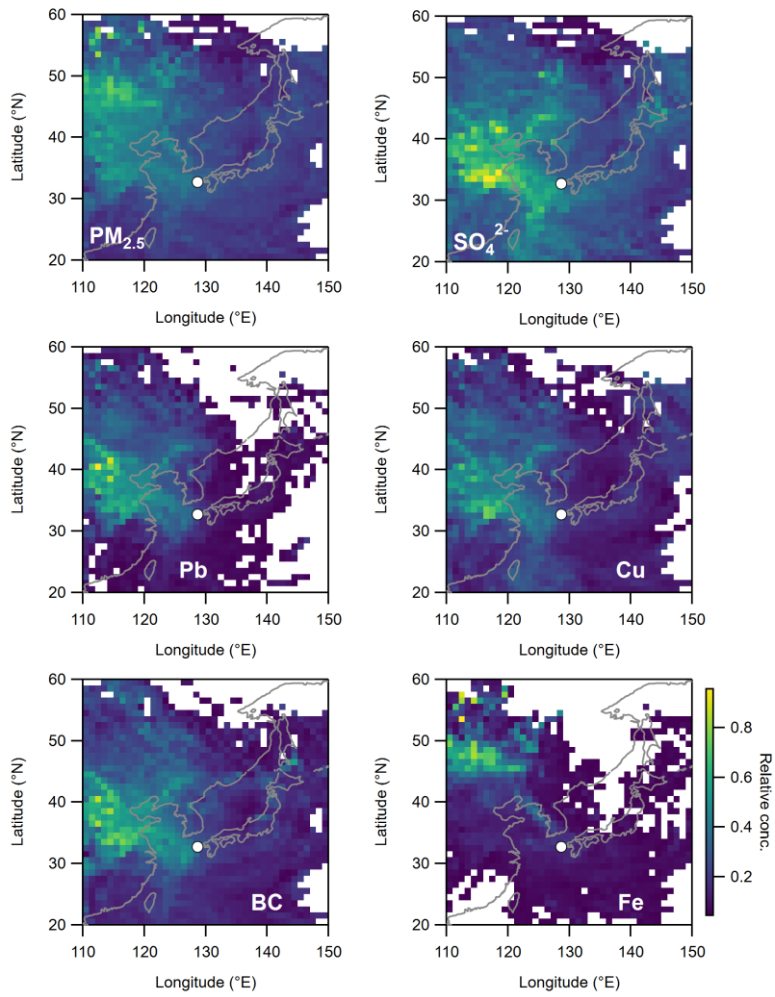
Figure 2. Concentration-weighted trajectories of PM$_{2.5}$, sulfate (SO$_4^{2-}$), Pb, Cu, black carbon (BC), and Fe during the study period. Color scales are adjusted to the same range of 10%–90% of their concentration values for all the plots. The location of Fukue Island is indicated by open circles.

750
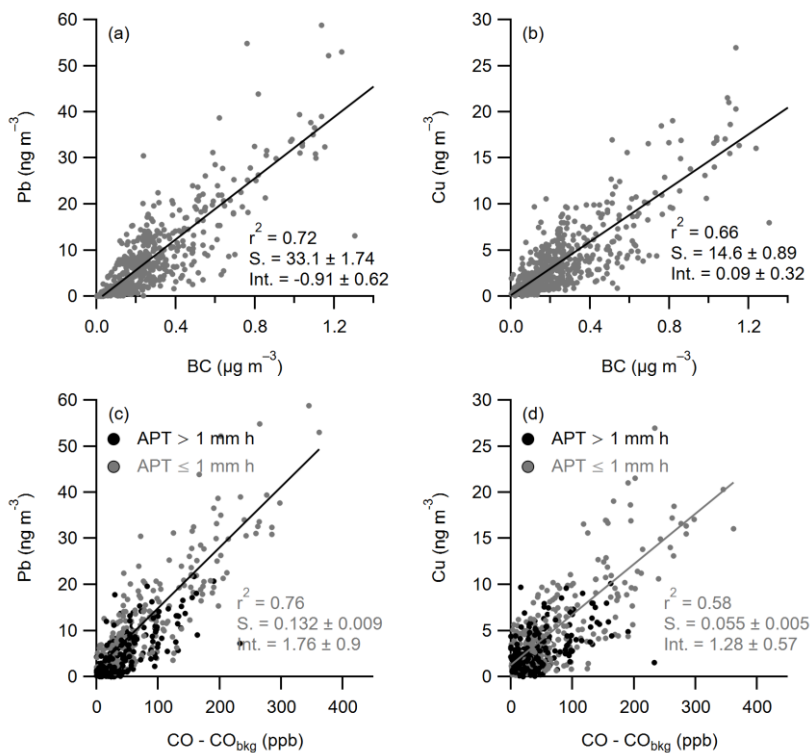
Figure 3. Correlations of black carbon (BC) with Pb (a) and Cu (b), and the enhancement of carbon monoxide above the background ($\Delta CO \equiv CO - CO_{bkg}$) with Pb (c) and Cu (d). In (c) and (d), the data points with the accumulated precipitation along trajectories (APT) higher than 1 mm h are highlighted as black circles.
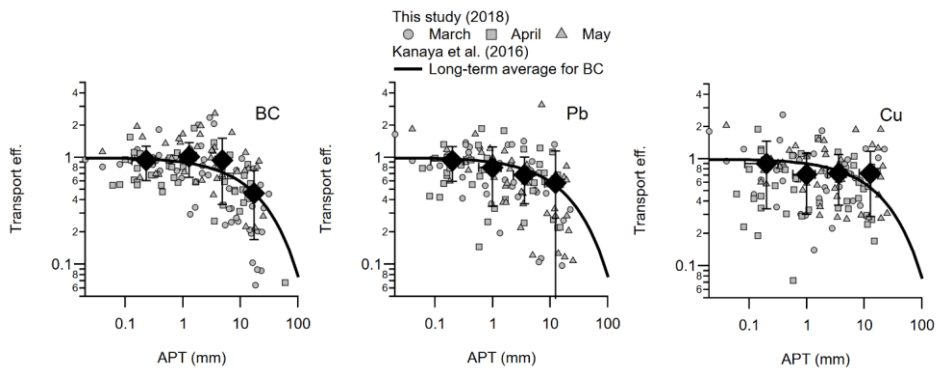
755

Figure 4. Transport efficiency for black carbon (BC) (left), Pb (middle), and Cu (right) as a function of accumulated precipitation along trajectories (APT) during the observation period. Shaded markers for 4-hourly data points are differentiated by the month (circles (March), squares (April), and triangles (May)). Filled black markers and error bars represent the binned averages and standard deviations. As a reference of the long-term tendency, the relationship between TE_{BC} and APT in East
760   Asia evaluated by our previous study (Kanaya et al., 2016) is overlayed in all the figures (solid lines).
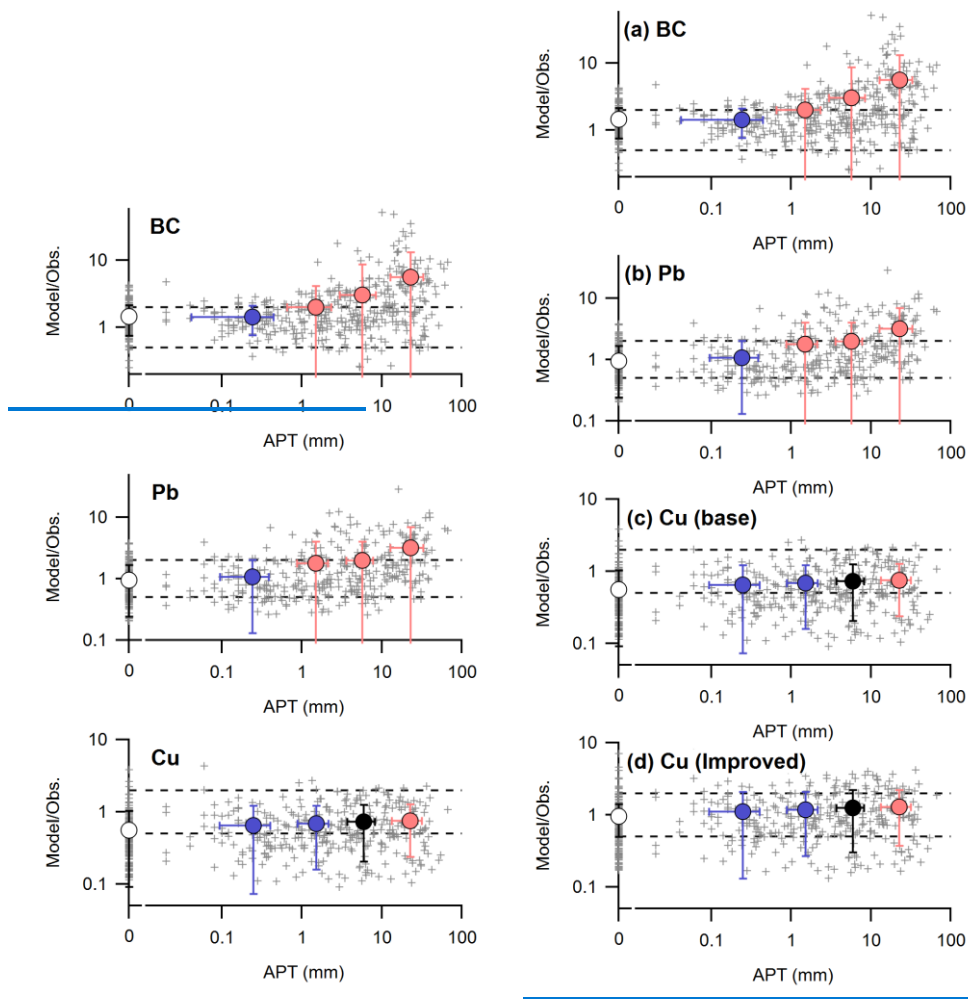
Figure 5. Model/Observed (M/O) ratios for (a) black carbon (BC) (top), (b) Pb (middle), (c) Cu (base simulation), and (d) Cu (bottomimproved simulation) as a function of the accumulated precipitation along trajectories (APT) during the observation period. Shaded cross markers represent all 4-hourly data points with data higher than the limits of detection of BC, Pb, and Cu.

Circles with the error bars are binned averages and standard deviations and are colored by the statistical significance of the differences in the M/O ratios from that at APT of 0 (student's t test results of $p < 0.01$ (red), $0.01 < p < 0.05$ (black), and $p > 0.05$ (blue)). The dashed lines depict the boundaries of factor of 2.
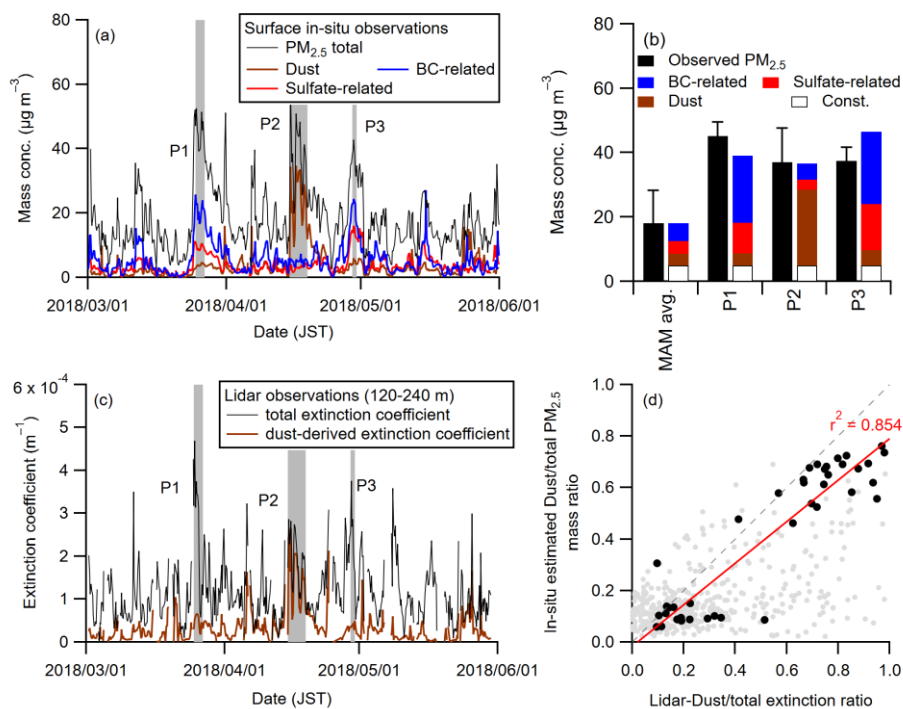
Figure 6. (a) Temporal variations of the observed $PM_{2.5}$ (black) and estimated BC-related $PM_{2.5}$ (blue), sulfate-related $PM_{2.5}$ (red), and dust-related $PM_{2.5}$ (brown) in Fukue Island. The selected periods when the Japanese air quality standard for the short-term (daily $PM_{2.5} > 35$ μg m^{-3}) was violated are highlighted by shaded areas. (b) Average observed concentrations of $PM_{2.5}$ (black bars) and those reconstructed using the tracers (colored bars: BC-related (blue), sulfate-related (red), dust (brown), and background (white)) for the entire period and selected periods (P1, P2, and P3). The error bars are standard deviations. (c) Temporal variations of the observed total extinction coefficient (black) and classified dust extinction coefficient (brown) at the altitude of 120−240 m in Fukue Island. (d) Correlation between the estimated contribution of dust to $PM_{2.5}$ mass and the lidar-derived contribution of dust to total extinction at the altitude of 120−240m (black for the selected periods (P1, P2, and P3) and shaded for other periods).

775

780
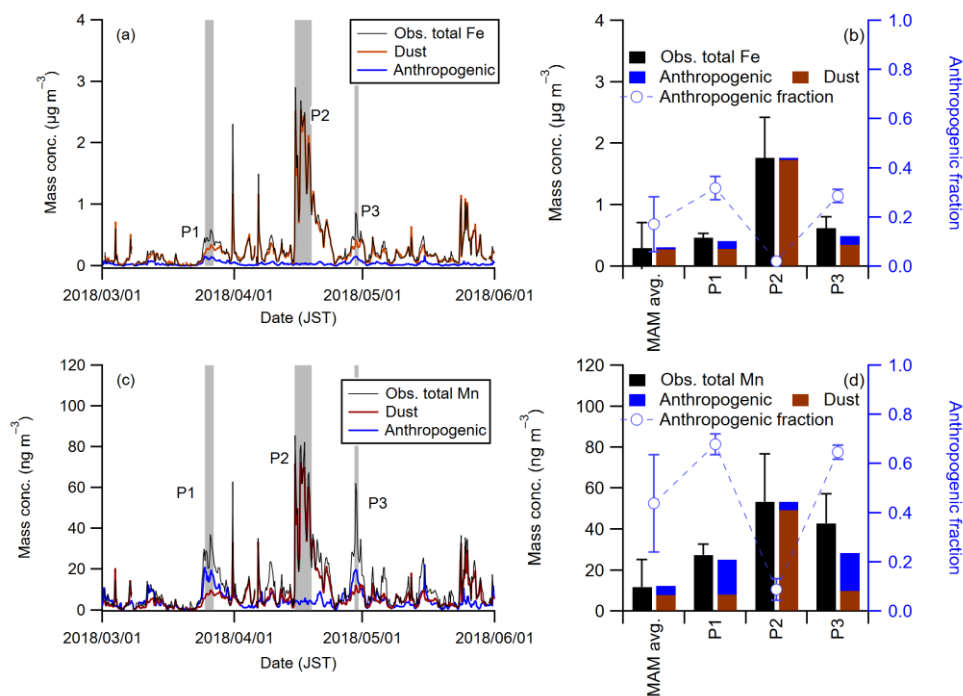
Figure 7. (a) Temporal variations of the observed Fe (black), and estimated anthropogenic Fe (blue), and dust Fe (brown) in Fukue Island. (b) Average observed concentrations of Fe (black bars) and those reconstructed using the tracers (colored bars: anthropogenic (blue) and dust (brown)) for the entire period and selected periods (P1, P2, and P3). The blue open markers and dashed lines are the estimated anthropogenic contribution to total Fe for the entire period and selected periods (P1, P2, and P3), respectively. (c) Temporal variations of the observed Mn (black), estimated anthropogenic Mn (blue), and dust Mn (brown) in Fukue Island. (d) Average observed concentrations of Mn (black bars) and those reconstructed using the tracers (colored bars: anthropogenic (blue) and dust (brown)) for the entire period and selected periods (P1, P2, and P3). The blue open markers and dashed lines are the estimated anthropogenic contribution to total Mn for the entire period and selected periods (P1, P2, and P3), respectively. The selected periods when the Japanese air quality standard for the short-term (daily $PM_{2.5} > 35$ µg m^{-3}) was violated are highlighted by shaded areas in (a) and (b). The error bars in (c) and (d) are standard deviations for the concentrations and the anthropogenic contributions.
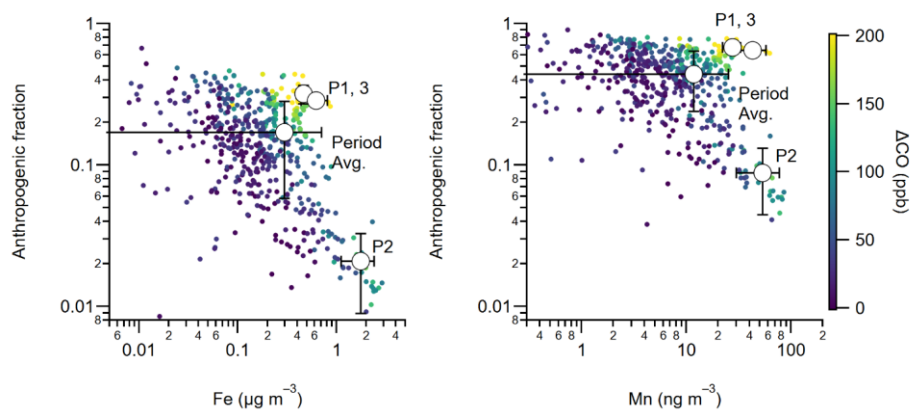
795 **Figure 8.** Relationship between the observed concentrations of Fe (left) and Mn (right) and their estimated anthropogenic contributions. The data points are colored by the values of the enhancement of carbon monoxide above the background ($\Delta CO \equiv CO - CO_{bkg}$). The open markers and error bars in the figure show the averages, standard deviations of the concentrations, and the anthropogenic contributions of Fe and Mn for the entire period and selected periods (P1, P2, and P3).

Supporting information for "Trace elements in $PM_{2.5}$ aerosols in East Asian outflow in the spring of 2018; Emission, transport, and source apportionment"

Takuma Miyakawa[1], Akinori Ito[1], Chunmao Zhu[1], Atsushi Shimizu[2], Erika Matsumoto[3], Yusuke Mizuno[3], Yugo Kanaya[1]

[1]Research Institute for Global Change, Japan Agency for Marine-Earth Science and Technology, Yokohama, 236-0001, Japan

[2]Regional Environment Conservation Division, National Institute for Environmental Studies, Tsukuba, 305-8506, Japan

[3]Horiba Ltd., Ohtsu, 520-0102, Japan

Correspondence to: Takuma Miyakawa (miyakawat@jamstec.go.jp)

This supporting information includes details of the multiple linear regression (MLR) model, and 11 13 figures, and 1 table.

S1. Source apportionment of $PM_{2.5}$ aerosols based on multilinear regression (MLR) analyses

In Sect. 3.5.1, MLR model was applied to the source apportionment of $PM_{2.5}$ aerosols using the temporal variations in concentrations of silica, black carbon, and sulfate ($[Si]_t$, $[BC]_t$, and $[SO_4^{2-}]_t$, respectively). Before determining the input variables for this analysis, several cases were tested based on the following equations:

$$[PM_{2.5}]_t = g_{Si} \cdot [Si]_t + g_{sulfate} \cdot [SO_4^{2-}]_t + C1 \qquad \text{(Eq. S1)}$$

$$[PM_{2.5}]_t = g_{BC} \cdot [BC]_t + g_{Si} \cdot [Si]_t + C2 \qquad \text{(Eq. S2)}$$

$$[PM_{2.5}]_t = g_{BC} \cdot [BC]_t + g_{Si} \cdot [Si]_t + g_{sulfate} \cdot [SO_4^{2-}]_t + C3 \qquad \text{(Eq. S3)}$$

The coefficients g_X (X = BC, Si, and sulfate) and C1–C3 (i.e., the constant term for the Eqs. (S1)–(S3)) were determined by the least squares method. The fitting residuals (i.e., chi square) for these cases were analyzed to diagnose the impacts of the input variables on the MLR model's performance. The values of chi square for the Eqs. (S1)–(S3) were determined to be 13936.2, 10166.6, and 8337.6, respectively. Putting these three components in the MLR model led to the minimum values of chi-square among these three cases. The comparison of the results between Eqs. (S1) and (S2) suggested that [BC] and [Si] can better account for $[PM_{2.5}]_t$ than $[SO_4^{2-}]$ and $[Si]_t$, indicating that $[BC]_t$ can be a tracer for not only primary anthropogenic emissions but also a part of secondary formation from the anthropogenic sources in this study. This was expected from the observed positive correlation between $[BC]_t$ and $[SO_4^{2-}]_t$ (**Figure S7**). As the value of $g_{sulfate}$ for Eq. (S3) was less than unity, the SO_4^{2-} related component cannot represent all the variations in the impacts of the secondary formations of inorganic (e.g., ammonium sulfate and nitrate) and organic aerosols (OAs). Thus, SO_4^{2-} related components can represent the aqueous phase production reaction of SO_4^{2-} and OAs in aerosol and cloud droplet phases. The value of C3 (4.95 µg m^{-3}) represents the background levels of $[PM_{2.5}]_t$ in East Asian outflow in the spring of 2018 and can include the sea salt (SS) aerosols emitted

from the ocean surface and some other secondary aerosols. In this study, the possible impacts of SS aerosols on the source apportionment of $PM_{2.5}$ aerosols were assessed using the temporal variations of chlorine concentrations $[Cl]_t$ in $PM_{2.5}$ aerosols, which were measured using the PX-375. As SS aerosols are chemically reactive and chlorine in SS can be removed by the reaction with acidic gases such as sulfuric acid, SS mass concentrations from the $[Cl]_t$ with the assumed seawater composition can be estimated as its lower estimate ($[SS_{MIN}]_t$). The SS_{MIN} contributed approximately 13% of $PM_{2.5}$ aerosol mass on average during the study period and was lower than C3, indicating that SS can account for almost half of the background level of $[PM_{2.5}]_t$ during the study period. The source apportionment of non-sea-salt components of $PM_{2.5}$ aerosols (nss-$PM_{2.5}$) was also analyzed in the same manner as follows:

$$[\text{nss-}PM_{2.5}]_t = [PM_{2.5}]_t - [SS_{MIN}]_t = g_{BC} \cdot [BC]_t + g_{Si} \cdot [Si]_t + g_{sulfate} \cdot [SO_4^{2-}]_t + C4 \qquad \text{(Eq. S4)}$$

The results for fitting the MLR models to the observed $PM_{2.5}$ and nss-$PM_{2.5}$ aerosols are summarized in Table S1. The sum of C4 and the average values of $[SS_{MIN}]_t$ (4.69 µg m^{-3}) were almost the same as C3, indicating that SS components had no substantial impacts on the source apportionment using Eq. (S3). Indeed, the changes in the contributions of dust to total $PM_{2.5}$ aerosols ($g_{Si} \cdot [Si]_t/[PM_{2.5}]_t$) among Eqs. 3 and 4 were small (only 4% differences). As Cl is not a perfectly adequate tracer for SS aerosols, we selected Eq. 3 for the base case calculations of the source apportionments of $PM_{2.5}$ aerosols.

Table S1. Results of the MLR analyses for the $PM_{2.5}$ aerosols using Eqs. (S3) and (S4)

Eqs.	Chi-square	g_{Si}	g_{BC}	$g_{sulfate}$	C3 or C4
S3	8337.6	4.62 (±0.29)	20.78 (±2.15)	0.66 (±0.12)	4.95 (±0.60)
S4	9021.7	4.79 (±0.30)	23.45 (±2.23)	0.56 (±0.12)	2.26 (±0.63)

*Values in the parentheses are 95% confidence intervals for the determined coefficients.

The source apportionment results using Eq. (S3) were compared with those simulated by the IMPACT model (Ito and Miyakawa, 2023). **Figure S8** depicts the temporal variations of the observed, estimated, and modeled mass concentrations of $PM_{2.5}$ total, dust, non-dust (i.e., anthropogenic and secondary formation), and SS aerosols. The mass concentrations of the observed $PM_{2.5}$ total and the estimated dust and non-dust aerosols agreed well with those simulated by the IMPACT model, indicating that the dust fraction of $PM_{2.5}$ aerosols was successfully classified using Si as a tracer of dust aerosols. The SS_{MIN} showed similar concentration levels to the SS model; however, the temporal variations of the SS_{MIN} were not well reproduced by the IMPACT model. This is likely because the sub-grid scale sea spraying affecting the observed SS concentrations cannot be well simulated by the IMPACT model, whose horizontal resolution was 2.0° × 2.5° (latitude × longitude). The average levels of SS_{MIN} (2.43±2.11 µg m^{-3}) and SS modeled (2.24±2.01 µg m^{-3}) were lower than C3. The difference can be accounted for by the other components, such as sulfate and secondary organic aerosols, which can be regionally homogeneous in the springtime East Asian outflow (e.g., Matsui et al., 2014).
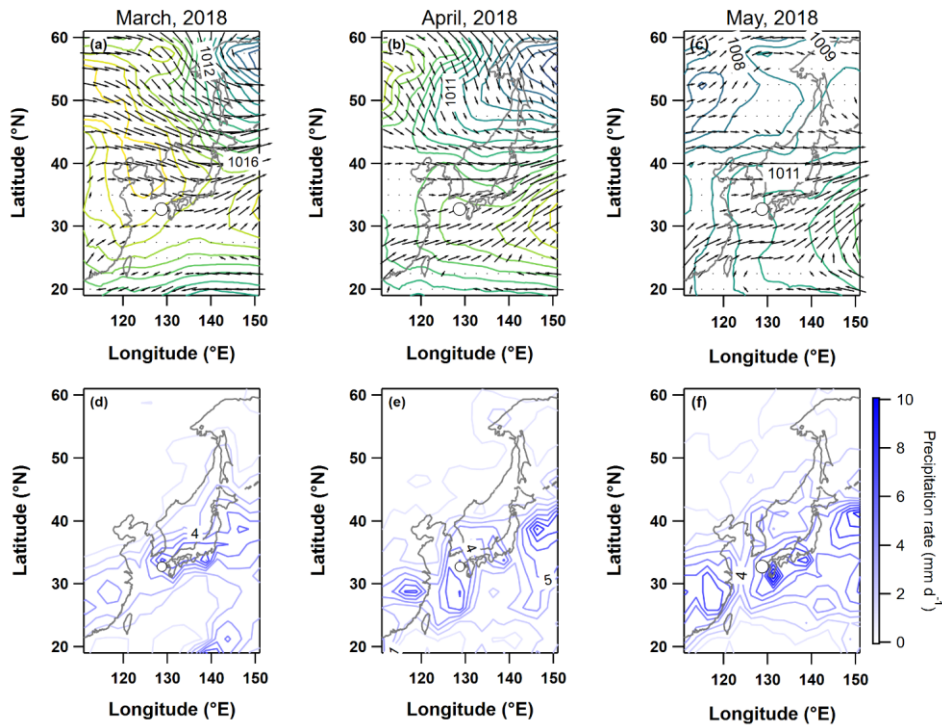
65 **Figure S1.** Monthly mean sea level pressure as contours and wind vectors at 850 hPa for (a) March, (b) April, and (c) May of 2018. Monthly mean precipitation rate for (d) March, (e) April, and (f) May of 2018. Monthly mean meteorological and precipitation data with a resolution of 1° in latitude and longitude were obtained from the National Centers for Environmental Prediction (NCEP) reanalysis and the Global Precipitation Climatology Project (GPCP), respectively.

70
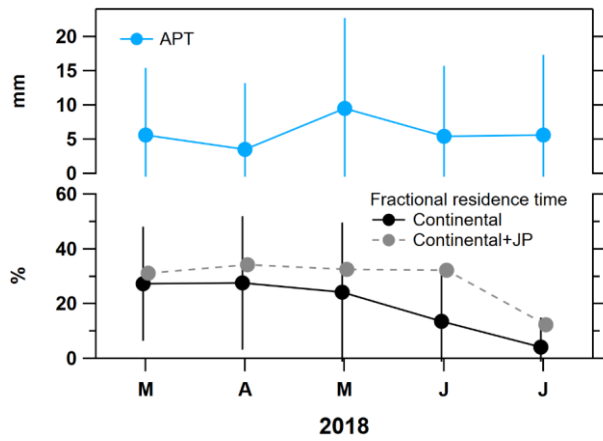
Figure S2. Seasonal progression of the monthly mean accumulated precipitation along trajectories (light blue markers and lines) in the top panel and the monthly mean fractional residence time over the continents (black markers and lines) and Japan (shaded markers and dashed lines) in the bottom panel. All the vertical bars represent the standard deviations of the monthly mean.
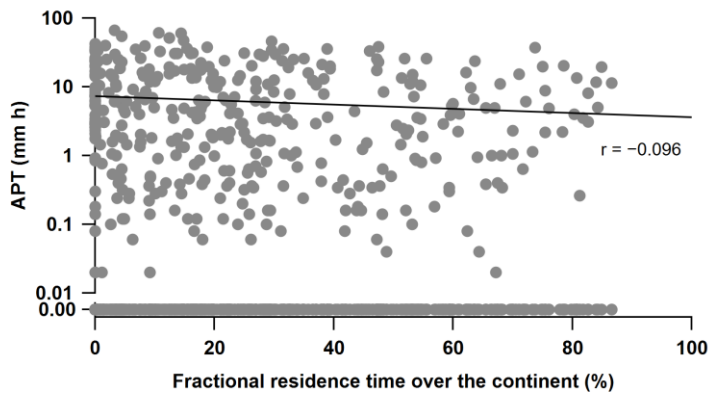
Figure S3. Relationship between the accumulated precipitation along trajectories and fractional residence time over the continent. The solid line depicts the linear regression line, which indicates that no significant correlation exists between the two parameters.
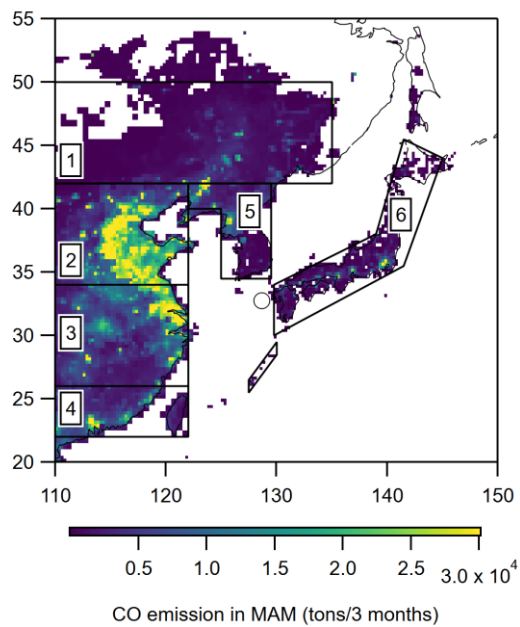
Figure S4. Anthropogenic carbon monoxide (CO) emission in the springtime (March–May, 2008) at East Asia from Regional Emission inventory in ASia (REAS v2.1) (Kurokawa et al., 2013). The encircled and labeled areas are considered for the calculations of fractional residence time (1: northeast China; 2: north central China; 3: south central China; 4 south China; 5: Korea; and 6: Japan). The East Asian continent is defined as the area labeled as 1–5.
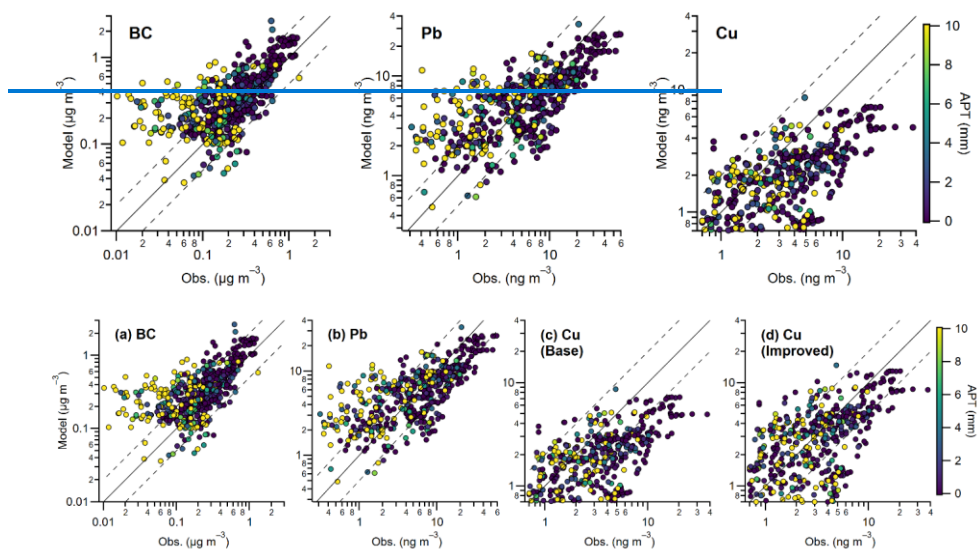
Figure S5. Correlations between the modeled and observed concentrations of (a) black carbon (BC) ~~(left)~~, (b) Pb ~~(middle)~~, (c) Cu (base simulation), and (d) Cu (~~right~~improved simulation) are colored by the values of the accumulated precipitation along trajectories. The solid line indicates the 1:1 line, and the two dashed lines indicate the boundaries of the factor of 2.
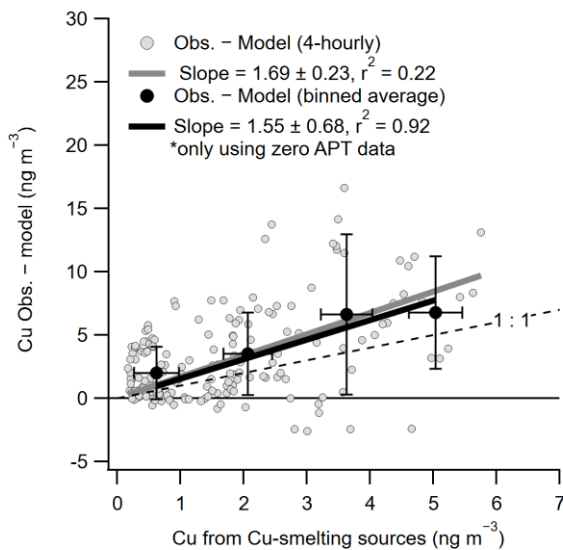
Figure S6. Correlation of the differences in Cu concentrations between observation and base model simulations (ΔCu) and the Cu concentrations from the Cu smelting sources ($Cu_{CuSmelt}$) when the accumulated precipitation along trajectories (APT) was zero (shaded and black closed markers for 4-hourly and binned-average data sets, respectively). The error bars depict the standard deviations of the binned data group of ΔCu and $Cu_{CuSmelt}$. The bold lines were calculated by linear regression analyses. Note that the fitted lines were calculated by forcing through the intercepts of zero. The dashed line depicts Y = X.
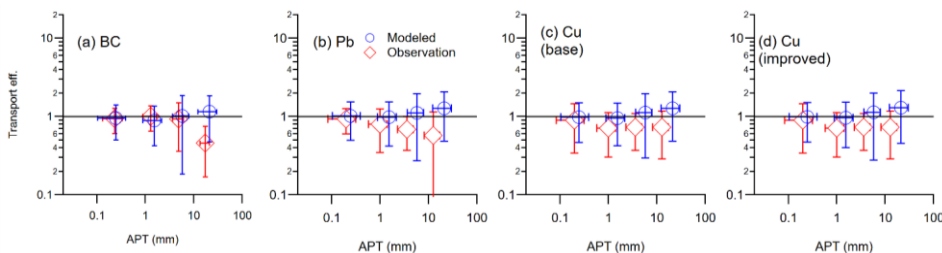
Figure S7. Relationship between the observation- (red) and model-based (blue) transmission efficiency (TE) for (a) BC, (b) Pb, (c) Cu (base simulation) and (d) Cu (improved simulation) and the accumulated precipitation along trajectories (APT). The binned average and standard deviations of the observed and modeled TE-APT data sets were plotted.
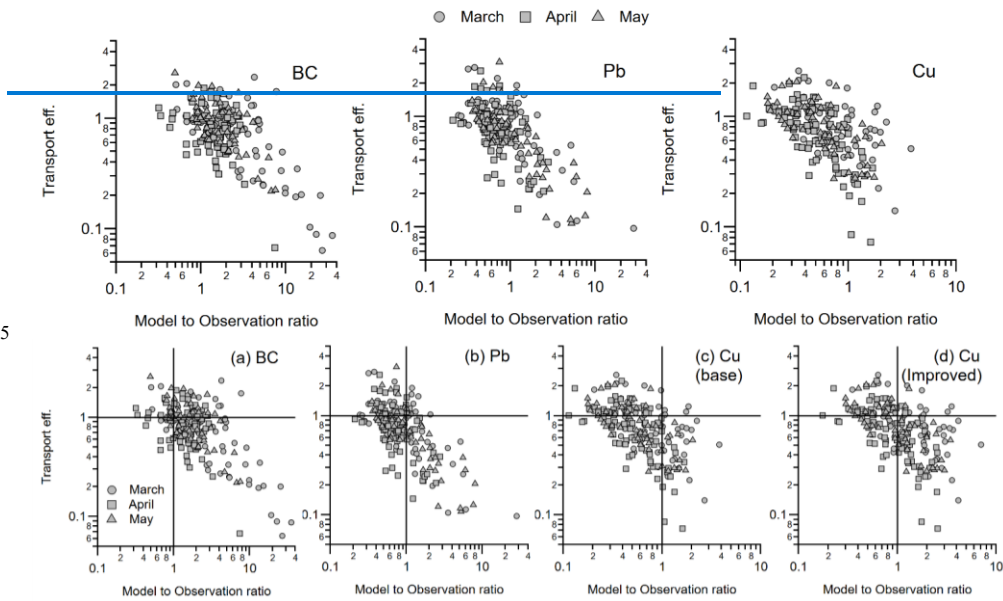
Figure S6S8. Relationship between the observed transport efficiency and model-to-observation ratios for (a) black carbon (BC) (left), (b) Pb (middle), (c) Cu (base simulation), and (d) Cu (improved simulationright). Shaded markers for 4-hourly data points are differentiated by the month (circles (March);), squares (April);), and triangles (May)) of 2018.
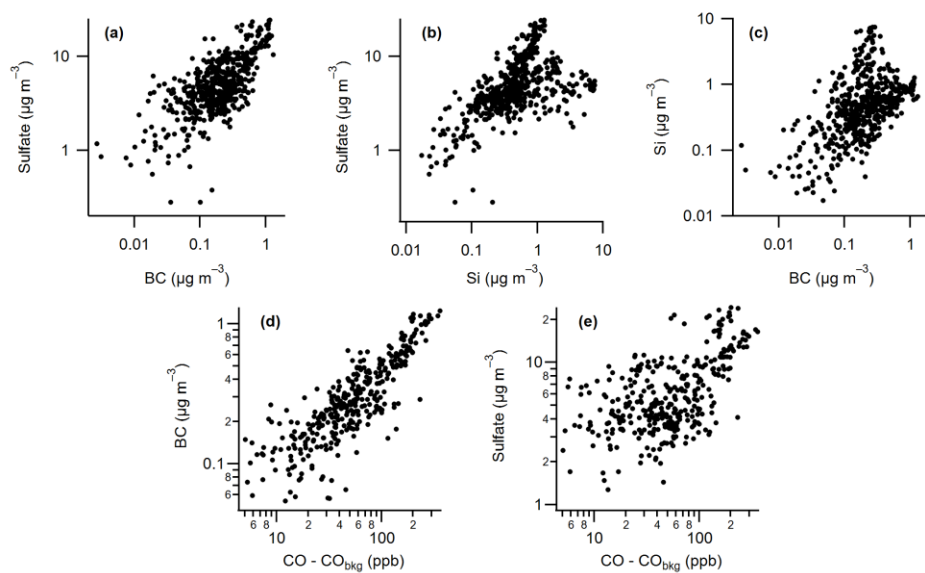
Figure ~~S7~~S9. ~~Correlations~~ Observed correlations of (a) black carbon (BC) and sulfate concentrations, (b) Si and sulfate concentrations, (c) BC and Si concentrations, (d) the enhancements of carbon monoxide (CO) from the background (ΔCO, see the main texts for the details) and BC concentrations, and (e) ΔCO and sulfate concentrations.

115
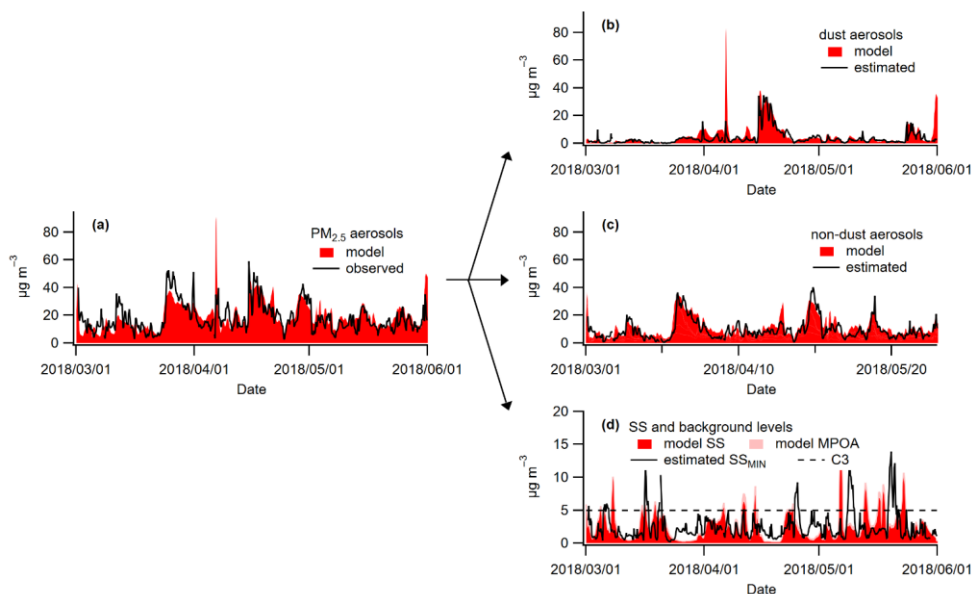
Figure S8S10. (a) Temporal variations in the modeled (red-filled area) and observed (black line) PM$_{2.5}$ aerosol concentrations. The temporal variations in the modeled (red-filled area) and estimated (black line) PM$_{2.5}$ dust (b) and non-dust (c) aerosol concentrations. The estimation was based on the equation S3 in Sect. S1 of this supporting information. (d) The temporal variations in the modeled (red-filled area) and estimated (black line) PM$_{2.5}$ sea salt (SS) concentrations. The modeled marine primary organic aerosol (MPOA, light red area) was stacked on the modeled SS in (d) to illustrate the modeled total concentrations of sea-spraying aerosols (SSA) and the contributions of MPOA to total SSA. The coefficient C3 in the MLR model using the equation S3 was also overlayed as the dashed line in (d).
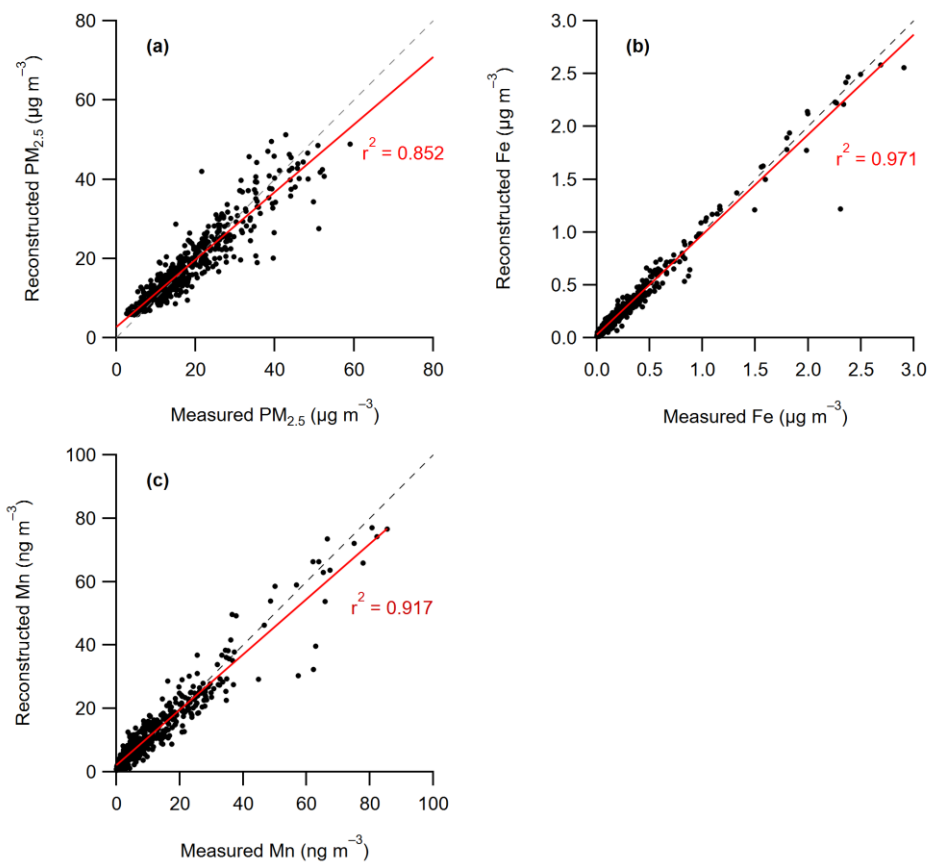
125

Figure S9S11. Correlations between the reconstructed and measured concentrations for (a) total $PM_{2.5}$ aerosols, (b) $PM_{2.5}$ Fe aerosols, and (c) $PM_{2.5}$ Mn aerosols. The dashed lines depict the 1:1 line, and red lines depict the linear regression lines for the correlations.
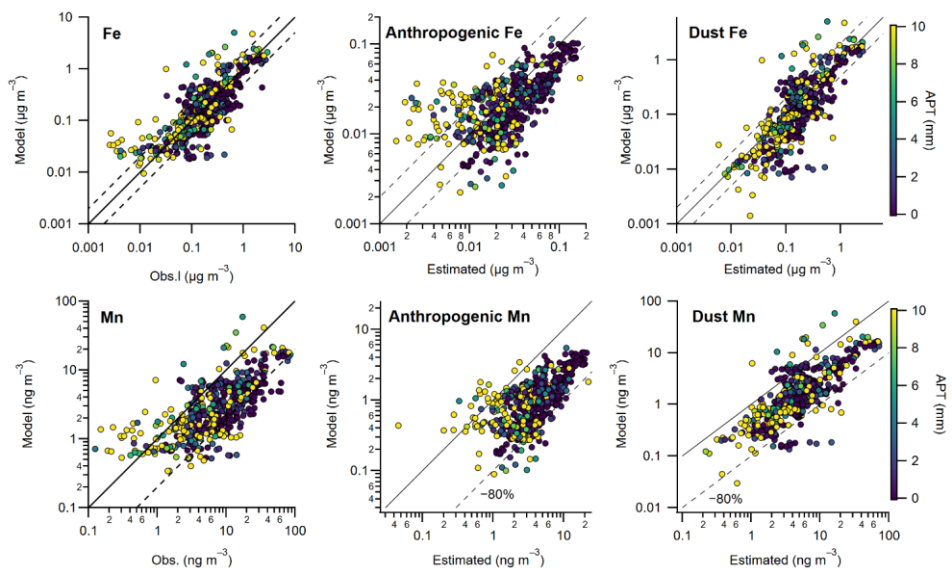
130

Figure ~~S10~~S12. (Top) Correlations of the modeled and observed/estimated concentrations of (left) total-Fe, (middle) anthropogenic-Fe, and (right) dust-Fe. (bottom) Correlations of the modeled and observed/estimated concentrations of (left) total-Mn, (middle) anthropogenic-Mn, and (right) dust-Mn. All the data points are colored by the values of the accumulated precipitation along trajectories (APT). The black line depicts the 1:1 line. The dashed two lines in the top panel depict the

135 boundaries of ~~the~~ factor 2. The dashed line in the bottom panel depicts the -80% of the model-to-estimation ratios.
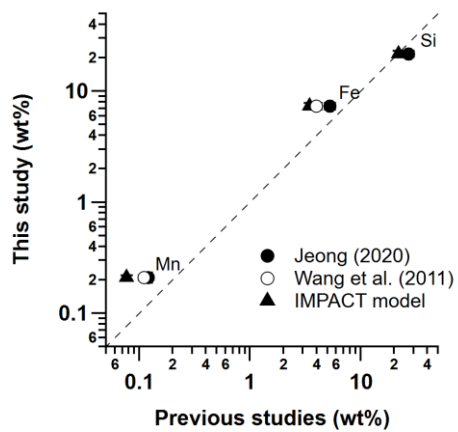
Figure S11S13. Comparison of the dust elemental compositions between this study and the other studies (filled circles: Jeong, 2020; open circles: Wang et al., 2011; triangles: modeled given in Ito and Miyakawa, 2023). The dashed line represents the 1:1 line.

References

Ito, A., and Miyakawa, T.: Aerosol iron from metal production as a secondary source of bioaccessible iron. Environ. Sci. &
145   Tech., 57(10), 4091–4100, https://doi.org/10.1021/acs.est.2c06472, 2023.

Jeong, G. Y.: Mineralogy and geochemistry of Asian dust: dependence on migration path, fractionation, and reactions with
         polluted air, Atmos. Chem. Phys., 20, 7411–7428, https://doi.org/10.5194/acp-20-7411-2020, 2020.

Kurokawa, J., Ohara, T., Morikawa, T., Hanayama, S., Janssens-Maenhout, G., Fukui, T., Kawashima, K., and Akimoto, H.:
         Emissions of air pollutants and greenhouse gases over Asian regions during 2000?2008: Regional Emission inventory in
150   ASia (REAS) version 2, Atmos. Chem. Phys., 13, 11019–11058, https://doi.org/10.5194/acp-13-11019-2013, 2013.

Matsui, H., Koike, M., Kondo, Y., Takami, A., Fast, J. D., Kanaya, Y., and Takigawa, M.: Volatility basis-set approach
         simulation of organic aerosol formation in East Asia: implications for anthropogenic biogenic interaction and
         controllable amounts, Atmos. Chem. Phys., 14, 9513–9535, https://doi.org/10.5194/acp-14-9513-2014, 2014.

Wang, Q., Zhuang, G., Li, J., Huang, K., Zhang, R., Jiang, Y., Lin, Y., and Fu, J. S.: Mixing of dust with pollution on the
155   transport path of Asian dust – revealed from the aerosol over Yulin, the north edge of Loess Plateau. Sci. Tot. Environ.,
         409(3), 573–581, https://doi.org/10.1016/j.scitotenv.2010.10.032, 2011.